

The Internal Kink Mode and Giant Sawteeth in Tokamaks

Dalton D. Schnack

March 5, 2012

1 Introduction

These rough notes are a result of my attempts to gain a rudimentary understanding of sawtooth oscillations in general, and giant sawteeth in particular. I have always learned best by writing down what I read: in going from printed page through brain to hand, perhaps some of it sticks. Simultaneously, I decided to learn a little LaTeX. The result is what you have here.

The initial motivation was to do simulations of the giant sawtooth crash with the NIMROD code. I quickly found that I was groping in the dark (still am), and in need of some background. Why am I so ignorant? Why wasn't I taught this stuff in graduate school? Actually, it turns out that much of the work on the topic was done *after* I left grad school and was involved in other endeavors. Ignorance is bliss, and, yes, I should have paid more attention at those endless APS meetings. In any case, I need some self-education, and these notes are a summary of most of the important papers regarding the topic of the internal kink mode in tokamaks, and its stabilization by energetic particles. I make no pretense at mastery or expertise or completeness. The fundamental MHD is difficult, I know very little about kinetic theory, and I have found the mathematics to be a stretch. As the mouse said: "Mine is a long and sad tail."

Here is a quick summary of what I've learned so far:

Sawteeth are the experimental manifestation of the $m = 1, n = 1$ internal kink mode in a torus. The sawtooth crash occurs when $q(0) < 1$. The ideal internal kink mode has completely different properties in a torus than in a periodic cylinder; it becomes pressure, rather than current, driven. Resistivity is required to account for the experimentally measured amplitude and growth rate of the sawtooth crash. In modern tokamaks, and in ITER, extended MHD or kinetic theory must be used to describe the singular layer; nonetheless the linear theory has been worked out.

Extended sawtooth-free periods with $q(0) < 1$ can be induced by the presence of an energetic ion population, from neutral beams and/or acceleration by RF radiation. These periods exhibit improved confinement properties and significant increases in stored energy. They are usually terminated by large sawtooth crashes, exactly like normal sawteeth except with much larger amplitude. These are “monster”, or giant, sawteeth. They can result in a rapid loss of stored energy and energetic particles, and can induce other MHD activity, like NTMs or ELMs. They may have serious negative implications for ITER.

The stabilization of the internal kink is due to an interaction between the toroidal precessional motion of the energetic trapped particles and low frequency MHD perturbations. The precessional motion of the banana centers of the trapped particles preserves the third adiabatic invariant, which is the magnetic flux linked by the precessing orbits. This can stabilize the kink mode if the particles complete many toroidal transits in an MHD growth time, i.e., $\gamma_I \ll \omega_p$. If γ_I and ω_p are not widely separated, a resonance between the MHD and the toroidal drift can destabilize fishbone mode. The trick is to have enough particles with enough energy to stabilize the kink without destabilizing the fishbone.

The theory of sawtooth stabilization by energetic particles is long and complex (if not actually sad). It has been synthesized into a simple analytic model, called the Porcelli model, that can be used to predict the triggering of a sawtooth crash. The Porcelli model uses zero-dimensional formulas based on a combination of theory and curve fitting to estimate the terms in the potential energy. The model has been tested by direct comparison with more extensive theory and experiment. The approximations used in the Porcelli model significantly underestimate the ideal MHD drive for the instability. When used with a more accurate (and expensive) computational estimate for the ideal MHD potential energy, the Porcelli model can be a useful guide to the prediction of the onset of a giant sawtooth crash.

Neither linear theory nor the Porcelli model can be used to predict accurately the state *after* the crash: e.g., what are the relaxed profiles?; what is the coupling to other MHD activity?; how much stored energy is lost?; where does it go?, and, what is the fate of the energetic particles? Addressing these questions requires *nonlinear* computations that employ self-consistent coupling between nonlinear extended MHD and a kinetic treatment of hot particles. These studies are beginning using the NIMROD code.

The presentation is organized as follows. Section 2 *briefly* reviews the first experimental observations of both normal and giant sawteeth. The development of the theory of the internal ink mode and its stabilization by energetic particles is discussed in Section 3. Section 3.1 is concerned with cylindrical geometry, including both linear and nonlinear ideal MHD theory, linear resistive and extended MHD theory, the ion-kinetic regime, and nonlinear computations. Section 3.2 discusses

the kink mode in toroidal geometry. The MHD behavior of the kink mode is completely modified. This is described in Section 3.2.1. The complicated theory of the effects of trapped particles, both thermal and energetic, on MHD activity is *very briefly* reviewed in Sections 3.2.2 - 3.2.6. A consolidated picture of linear kink mode behavior in a torus is described in Section 4, including a comprehensive theory of kink stabilization by energetic particles, Section 4.1, and a review of the Porcelli model for predicting the sawtooth trigger, Section 4.2. Comparison of both general theory and the Porcelli model with experiment is described in Section 4.3, and some thoughts on future directions, including some preliminary results from NIMROD, are presented in Section 4.4.

The presentation is rough and uneven (even redundant grammatically!). This is because the composition was done in a stream-of-consciousness fashion as I was trying to work through the papers. The notation is inconsistent because I have used the notation in the original papers; it changes from section to section. The papers are difficult, and I had more background (and patience) for some than for others.

Of course, I am looking for feedback, not in style but in content. There are several places where I admit ignorance and plead for assistance. I would sincerely appreciate comments and suggestions for improving both the accuracy and my understanding. Some examples are:

How do you derive Eq. (56), which is a critical step in the theory of the resistive internal kink?

Is there an easy way to understand the ion-kinetic regime, Section (3.1.5), or is it all just an endless series of approximations to gamma- and confluent hypergeometric functions?

Ditto for Kruskal-Oberman theory, Section 3.2.3. I can't see any connection between the original paper and the formulas used in the Porcelli model. And how would you include these effects in NIMROD?

How did White, Romanelli and Bussac work out all those formulas (see Section 4.1)? I am in awe!

Where does Eq. (121) come from?

Where does Eq. (133) come from?

Is a tail of high energy ions necessary for internal kink stabilization, or can it be achieved with a slowing down distribution (see Section 4.3)?

And, last but far from least, What are we going to do without Marshall Rosenbluth?

Anyway, even if you don't have the answers, I hope you find the notes useful.

2 Experiment

Sawtooth oscillations seem to occur naturally in all toroidal confinement configurations: tokamaks, RFPs, and spheromaks. They consist of quasi-periodic signals appearing in the data from a variety of experimental diagnostics. These signals are characterized by a slow rise followed by a fast “crash”. They were first reported in tokamaks (with which we are concerned here) in the early 1970’s, and have been seen in every tokamak since. Later, in the 1980’s, tokamak experimentalists learned how to stabilize these oscillations, leading to long “sawtooth-free” periods of improved confinement. Unfortunately, these were inevitably terminated by large sawtooth crashes (called “monster”, or “giant” sawteeth) that had adverse implications for the operation of a fusion reactor.

In this section the early experimental evidence for both normal and giant sawteeth is briefly reviewed. (It should be noted that an excellent review of sawtooth data and results has been given by Jardin [1].)

2.1 Sawtooth Oscillations

The first published report of sawteeth was in 1974 by von Goeler, Stodiek, and Sautoff [2] in the ST tokamak. They reported “sawtooth-like” oscillations in the x-ray signal from the core of the discharge, which is primarily a measure of the electron temperature. On the magnetic axis ($r = 0$), these oscillations had a slow rise phase and a rapid crash phase. At $r = 3.9$ cm. the oscillations were “inverted”, with a rapid rise followed by a slow decay. A sketch of the experimental arrangement and the x-ray signals are shown in Fig. 1. The sawteeth are the relatively rapid oscillations imposed upon the overall signal. Note that this span of < 100 mseconds represents the total duration of the discharge, illustrating the progress in tokamak confinement over the last 35 years. Apparently this type of oscillation had also been seen in the T-4 tokamak in Russia, and on the ATC tokamak at Princeton, but had not been reported in the open literature. (Reference [2] cites an unpublished Kurchatov Institute report by Vershkov, et al., and an unpublished PPPL report by R. R. Smith.) At the time, sawteeth were also called “internal disruptions”, which were disturbances limited to the core of the plasma. This is to distinguish them from “major disruptions”, which resulted in premature termination of the discharge.

In a tokamak like ST, the “safety factor” $q(r) \sim rB_z/RB_\theta$ (to use the cylindrical approximation) is a monotonically increasing function of the minor radius r . Prior to the crash the value of $q(0)$, the value of the safety factor on the magnetic axis, was estimate to be ~ 0.8 , with $q = 1$ occurring at $r \sim 2$ cm. Measurements showed that the sawtooth amplitude had a node at the $q = 1$ surface: inside this surface the temperature behaves like the lower trace in Fig. 1; outside, it behaves like the

upper trace (i.e., it is “inverted”). Thus, at the crash, the temperature inside the $q = 1$ surface exhibits a rapid decrease, while outside that surface it exhibits a rapid increase: the temperature profile flattens “outward” in minor radius. After the crash the temperature within the $q = 1$ surface slowly increases, while outside it slowly decreases, becoming more peaked until another crash and flattening occurs. The oscillations were also measured to be associated with helical perturbations having poloidal mode number $m = 1$ and toroidal mode number $n = 1$, which were theoretically known to be characteristic of the internal kink mode [3, 5], an ideal MHD instability that occurs in the vicinity of the $q = 1$ surface.

The following theoretical picture sawtooth oscillations was given. The temperature profile begins the cycle relatively flat, and $q(0) > 1$, as required for ideal stability. The plasma is heated ohmically (i.e., by collisions that resist the plasma current). Since the current density is peaked on axis ($q(r)$ is monotonic in r), the core of the plasma is preferentially heated, causing the temperature to peak in the core. Since the resistivity decreases with increasing temperature ($\eta \sim T^{-3/2}$ for a collisional plasma), the core becomes a relatively better electrical conductor than the edge, and the current density further peaks at $r = 0$, causing $q(0)$ to decrease. This leads to a further increase in the local heating rate, a further peaking of the temperature, and a further decrease in $q(0)$. Finally $q(0) < 1$, and the internal kink instability ($m = 1, n = 1$) is triggered. Its nonlinear evolution leads to a rearrangement of the magnetic flux and a flattening outward of the temperature,

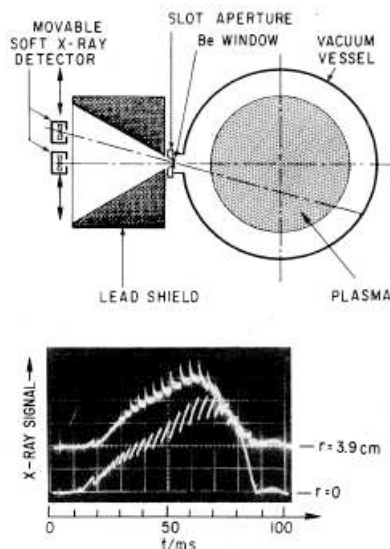


Figure 1: Experimental setup and x-ray signals showing sawtooth oscillations in the ST tokamak [2].

until the original state with relatively flat temperature and $q(0) > 1$ is restored. The cycle then repeats.

A theoretical picture of the linear and nonlinear properties of the ideal MHD internal kink mode was given in Ref. [5]. (It is interesting that Ref. [5] was actually published *before* the experimental results reported in Ref. [2]. Is this a case, unusual for plasma physics, of theory leading experiment?) In particular, Ref. [5] provided an estimate of the saturated amplitude of the mode (see Section 3.1.2, below). In the ST tokamak [2], the growth rate of the mode responsible for the sawtooth oscillations was estimated to be smaller (by a factor of 8) and the amplitude of the mode larger by about an order of magnitude than the estimates of Ref. [5]. “It should be pointed out that resistivity is not included in the present theory and that it is likely that a tearing-mode version of this instability exists which might lead to smaller growth rates and larger displacements.” [2] This is indeed the case, as will be seen in subsequent sections.

A more detailed model of sawtooth oscillations, including the rearrangement of the flux due to magnetic reconnection, was given by Kadomtsev [6].

Of course, it has since become known that sawtooth oscillations, or “internal disruptions”, are a characteristic and ubiquitous part of tokamak operation. As was pointed out by Furth (see the discussion section of Ref. [7]): “Disruptive instabilities are of great physical interest, but tokamak experiments can readily be operated in a way that avoids gross disruptions, and this is the normal operating mode. Furthermore ... there are regimes that are entirely free of both major and minor disruptions, and indeed of any kind of marked MHD activity. From a theoretical point of view, this can be explained by introducing finite-temperature stabilizing terms into resistive MHD theory. In addition, it has been shown recently that there exist altogether stable special tokamak profiles, even without the benefit of finite-temperature stabilizing terms.” It all seems so simple.

2.2 Giant Sawteeth

We have seen that sawtooth oscillations are a ubiquitous signature of tokamak operation. As might be expected (and in spite of Furth’s remarks [7]), the repeated collapse of the central electron temperature and the resulting mixing of the plasma between the core and the outer regions has an adverse effect on plasma confinement (during the crash the core is, by definition, unconfined), and, in a fusion reactor, may lead to ejection of the energetic charged particles (α -particles) that result from fusion reactions and are an integral part of the energy balance requirements. These adverse effects on tokamak performance led to attempts to find ways to control, and possibly stabilize and eliminate, sawtooth oscillations.

The first reported progress in this regard was on the JET tokamak [8]. They reported the inducement of extended sawtooth-free periods in response neutral

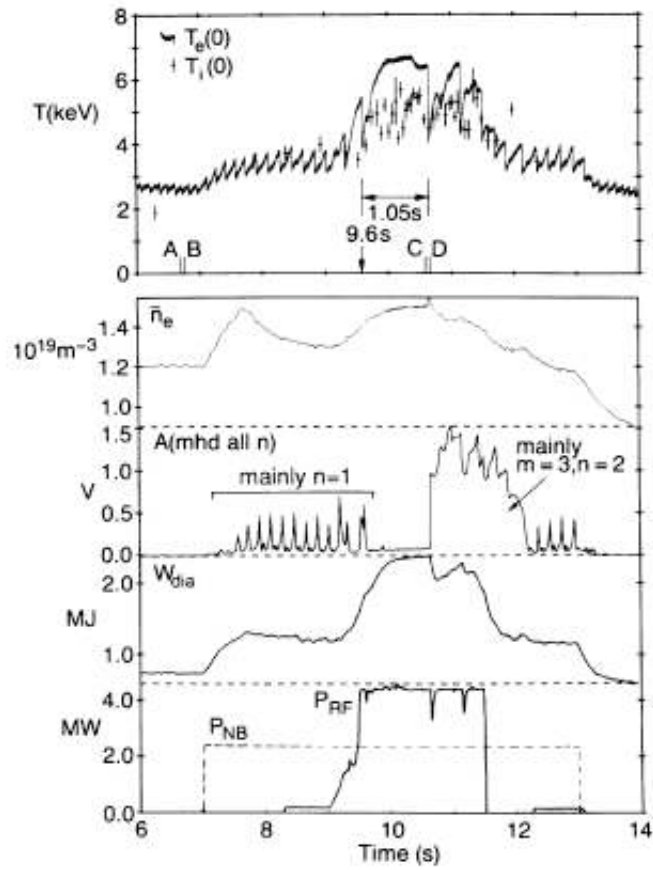


Figure 2: Data from the JET tokamak showing the onset of a sawtooth-free period at 9.6 seconds in response to neutral beam injection and ICRF heating. The stable period lasted 1.05 seconds. [8].

beam injection followed by RF (ICRH) heating. The RF accelerates the beam ions to energies of several hundred KeV. An example is shown in Fig. 2. The stable period starts at 9.6 seconds, and lasts 1.05 seconds. The preceding and subsequent oscillations are normal sawteeth. During the sawtooth interregnum, the temperature and stored energy approximately doubled, the confinement time improved by up to 20 percent, and $q(0)$ was maintained well below unity. During this time there was little or no detectable MHD activity.

The sawtooth-free period was terminated by an $m = 1, n = 1$ instability, followed by $m = 2, n = 1$ and $m = 3, n = 1$ activity; $q(0)$ was returned to greater than one. It is in all respects a “normal” sawtooth crash, except with much larger amplitude. This is the first report of what later became known as a “monster”, or “giant” sawtooth. One might think that a large amplitude MHD event that results in the loss of half the stored energy and stimulates other MHD activity throughout the discharge might be cause for some concern, although Ref. [8] does not seem to find it remarkable. The paper stresses the stabilization and the improved confinement, minimizes (or ignores) the implications of the crash, and seems (to me) to be naively (or, perhaps, politically) optimistic about the results. Subsequent experience (see, for example, Ref. [9], and references therein) showed that giant sawteeth could trigger both ELMs and neo-classical tearing modes (NTMs), dump large amounts of energy to the walls, and cause significant loss of energetic particles (such as α -particles in a fusion reactor). Normal sawteeth are like a slow leak in a tokamak. If they are eliminated it allows energy to build to the point where its sudden release could have serious consequences for both confinement and structural integrity. A giant sawtooth could be a significant event for ITER.

Of course, the physics question is: what causes the stabilization of the $m = 1, n = 1$ kink mode? Experimentally their stabilization (and, as we shall see, other unexpected MHD-like activity) is associated with a minority population of energetic ions that, in the low collisionality regime of modern tokamaks, can become “trapped” on the outboard side of the torus. These ions can come from a neutral beam, or from fusion reactions. They can be accelerated to higher energy by RF radiation. It turns out that the interaction between these ions and low frequency MHD activity can completely alter the MHD stability properties of a toroidal plasma. The analysis is extremely complex, and requires a fusion (pardon the pun) of MHD and kinetic theory. However, smart people were eventually able to show that, under the proper circumstances, the presence of these energetic particles can, indeed, lead to complete stabilization of the internal kink mode. This will be described in the following sections.

All of the theoretical progress has been made with the goal of understanding the *linear* theory of kink stabilization, thereby determining the so-called “trigger

mechanism” for the giant sawtooth. As stated, and as we shall see, this is a difficult task. However, it cannot address the *real, practical* consequences of a giant sawtooth crash: the loss of stored energy, the load on the walls and supporting structure, the triggering of other unstable MHD modes, the fate of the energetic ion population, etc. These are all determined by the *nonlinear* evolution of the internal kink mode in a torus in the presence of an energetic ion population, and ultimately can only be addressed by large scale numerical simulation. Initial steps in this direction are briefly described in Section 4.4.

3 Theory

We now proceed to review the linear and nonlinear theory of the internal kink mode, which is responsible for the sawtooth crash. The simplest geometry in which to study this mode is a periodic cylinder, and there are two principal results. First, in ideal MHD the growth rate is small ($\gamma \sim \epsilon^2$, where $\epsilon = r/R \ll 1$ is the cylindrical equivalent of the aspect ratio of a torus). The second is that, in the absence of resistivity, the saturation amplitude of the kink is also small ($\xi \sim \epsilon^2$), so that the ideal internal kink cannot account for the observed sawtooth crash. This later restriction is removed in resistive MHD theory, and the resistive kink mode can completely rearrange the flux in the core. This is described in Section 3.1.

Unfortunately, tokamaks are tori, not cylinders, and the toroidal corrections to the theory are also $\sim \epsilon^2$, which is the same order as the growth rate. It turns out that the linear stability properties of the kink are not just modified by toroidal geometry, but are completely changed, so that the cylindrical theory cannot be used to make reliable predictions. But that all gets worked out, and is described in Section 3.2. It is the toroidal resistive internal kink (and its modifications when the collisionality becomes very small) that is responsible both normal and giant sawtooth crashes.

As suggested in Section 2.2, the stabilization of the internal kink mode in a torus is the result of an interaction between MHD and energetic trapped particles. This complex theory is described briefly in Sections 3.2.4 and 3.2.6.

Of course, all of what follows is to be considered in the context in which it is presented: notes written following a brief perusal of some of the most difficult papers in plasma physics. Have patience.

3.1 Cylindrical Geometry

3.1.1 Linear Ideal MHD

We first consider the case of ideal MHD linear stability in cylindrical geometry. In this case, Ohm's law is

$$\mathbf{E} = -\mathbf{V} \times \mathbf{B}, \quad (1)$$

where \mathbf{E} is the electric field, \mathbf{B} is the magnetic field, and \mathbf{V} is the fluid velocity. Equation (1) is a statement that a fluid particle moving with velocity \mathbf{V} sees no electric field. Equivalently, in a frame at rest in the laboratory, the electric field parallel to \mathbf{B} vanishes. In either case, the interpretation is that the fluid and the magnetic field are co-moving.

Perturbations behave as $e^{\gamma t} e^{(im\theta + k_z z)}$. For kink modes, the poloidal mode number is $m = 1$, and the axial wave number $k_z = n/R$, where n is an integer and R is the major radius of the "equivalent" torus. The so-called internal kink mode has $n = -1$, so the axial mode number is $k_z = -1/R$. The first complete analysis of the stability of this mode seems to be by Shafranov [3]. It is reviewed by Rosenbluth, Dagazian, and Rutherford[5]. They state that the analysis is "well known", but they do not give a reference. It is also discussed in some detail in Freidberg's book [10].

In Freidberg's notation[10, pp 289ff., 340ff., 419ff.], the potential energy per unit length of a periodic cylindrical plasma with conducting wall at radius a , subject to a perturbation ξ , is

$$\frac{\delta W}{2\pi R} = \frac{\pi}{\mu_0} \int_0^a \left[f \left(\frac{d\xi}{dr} \right)^2 + g\xi^2 \right] dr, \quad (2)$$

where

$$f = \frac{rF^2}{k_0^2}, \quad (3)$$

$$g = 2\frac{k_z^2}{k_0^2} (\mu_0 p)' + \left(\frac{k_0^2 r^2 - 1}{k_0^2 r^2} \right) rF^2 + \frac{2k_z^2}{rk_0^4} \left(k_z B_z - \frac{mB_\theta}{r} \right) F, \quad (4)$$

$$k_0^2 = \frac{m^2}{r^2} + k_z^2, \quad (5)$$

and

$$F = \mathbf{k} \cdot \mathbf{B} = \frac{mB_\theta}{r} + k_z B_z. \quad (6)$$

For the internal kink, $k_0^2 = k_z^2 + 1/r^2$ and

$$F = \frac{B_\theta}{r} (1 - q), \quad (7)$$

where $q = rB_z/RB_\theta$ is the safety factor. The resonant (or “rational”) “surface” (or radius) r_0 is defined as the root of $F(r_0) = 0$, or $q(r_0) = 1$. On this surface the wave fronts of the perturbation are parallel to the magnetic field. The internal kink occurs if r_0 lies within the plasma, i.e., $0 < r_0 < a$. If $q(r)$ is a monotonically increasing function of r , as is the usual case for a tokamak, then we have $F > 0$ for $r < r_0$, and $F < 0$ for $r > r_0$. The appearance of the internal kink resonance requires $q(0) < 1$ and $q(a) > 1$.

We will use the “tokamak ordering”, which can be expressed as $r/R \sim B_\theta/B_z \sim k_z r \sim \epsilon$ where $\epsilon \ll 1$ is a small parameter. The pressure can be ordered either as ϵ^2 (the standard ordering) or ϵ (the high- β ordering). For the internal kink mode ($m = 1, k_z = -1/R$), Equation (4) can be written in terms of q to $O(r^2/R^2) \sim \epsilon^2$ as

$$g = \frac{r^2}{R^2} [(1 - q)^2 - 2(1 + q)(1 - q)]. \quad (8)$$

Clearly, $g = 0$ at the rational surface $q = 1$. It is easy to show that $g < 0$ for $r < r_0$ and $g > 0$ for $r > r_0$.

We now consider the minimization of the potential energy, Equation (2). The first term in the integrand is positive definite, and the second term depends on the sign of g . A trial function that minimizes δW is therefore

$$\xi = \begin{cases} \xi_0 & \text{for } r < r_0, \\ 0 & \text{for } r > r_0. \end{cases} \quad (9)$$

The subscript 0 refers to the fact that ξ_0 is to be considered $O(1)$. This function, and typical current and safety factor profiles, are shown in Figure (3), which is taken from Ref [5]. The ideal MHD potential energy for this trial function is

$$\delta W_c = \frac{2\pi^2 R \xi_0^2}{\mu_0} \int_0^{r_0} g dr. \quad (10)$$

Since $g < 0$, $\delta W < 0$ and the internal kink is unstable. Note, however, that $\delta W \sim \epsilon^2$, so that the growth rate is expected to be correspondingly small.

The trial function given by Equation (9) has a singular derivative at $r = r_0$. This singularity is resolved by inertia at $O(\epsilon^2)$. Since the growth rate is $O(\epsilon^2)$, we expect the plasma to be in quasi-equilibrium everywhere except near the rational surface. That is, the inertia can be neglected everywhere except in a small region of width $r - r_0 = x \sim \epsilon^2$ about $r = r_0$. In that region the full equations must

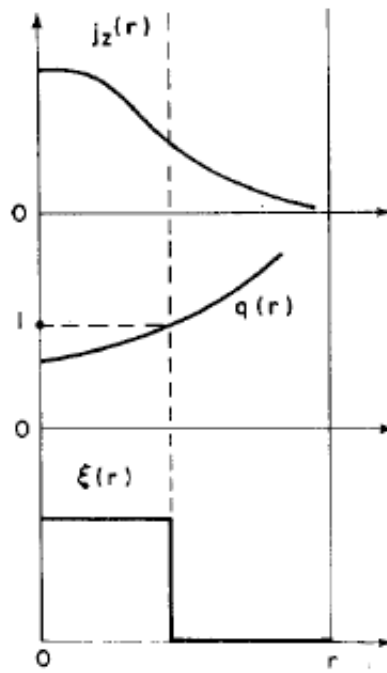


Figure 3: Tokamak profiles and the minimizing trial function

be solved. The growth rate is obtained by matching the solutions in the inner and outer regions at $r = r_0$. The correction to the displacement that resolves the singularity is $O(\epsilon^2)$.

The total energy is $E = K + \delta W$, where K is the kinetic energy in the poloidal flow. (In the tokamak ordering, the magnetic field is almost axial, and the parallel flow can be ignored[5].) Minimizing the total energy for incompressible displacements leads to the Euler equation

$$\frac{d}{dr} \left[(\mu_0 \rho \gamma^2 + F^2) r^3 \frac{d\xi}{dr} \right] - g\xi = 0 \quad (11)$$

where γ is the growth rate.

As mentioned above, the solution is divided into two parts: an “outer” solution away from the rational surface where inertia can be ignored, and an “inner” solution valid near the rational surface where inertia must be included. The solution in the outer region is then further divided into two parts: one valid for $0 \leq r < r_0$ and denoted as $\xi_{<}$, and one valid for $r_0 < r \leq a$, denoted as $\xi_{>}$. To obtain the outer solution, we set $\gamma = 0$ and integrate over the two parts of the outer region. We use the *ansatz* $\xi = \xi_0 + \epsilon^2 \xi_2$ (where ξ_0 is given by Equation (9)), and note that $g \sim O(\epsilon^2)$. Integrating from 0 to r , where $r < r_0$, we have

$$\frac{d\xi_{2<}}{dr} = \frac{\xi_0}{F^2 r^3} \int_0^r g(r') dr' , \quad (12)$$

This gives the slope of the outer solution in the region $0 \leq r < r_0$. Similarly, the slope of the outer solution in the region $r_0 < r \leq a$ is found by integrating from r_0 to r , where $g = 0$:

$$\frac{d\xi_{2>}}{dr} = \frac{C}{F^2 r^3} , \quad (13)$$

where C is a constant of integration, and we have used the fact that $F(r_0) = 0$.

The “inner” solution ξ_{in} is found by substituting $x = (r - r_0)/\epsilon^2$ into Equation (11) and retaining terms up to $O(\epsilon^2)$. The result is

$$\frac{d}{dx} \left[(\mu_0 \rho \gamma^2 + F'^2 x^2) r_0^3 \frac{d\xi_{in}}{dx} \right] = 0 , \quad (14)$$

where we have written $F(x) = F'x$. (The term $g\xi$ is $O(\epsilon^6)$ and is dropped.) Integrating twice, we have

$$\xi_{in}(x) = \frac{C_1}{r_0^3 \gamma |F'| \sqrt{\mu_0 \rho}} \tan^{-1} \frac{|F'|x}{\gamma \sqrt{\mu_0 \rho}} + C_2 . \quad (15)$$

The integration constants are found by requiring $\xi_{in} \rightarrow \xi_0$ as $x \rightarrow -\infty$, and $\xi_{in} \rightarrow 0$ as $x \rightarrow \infty$. The result is

$$\xi_{in} = \frac{1}{2}\xi_0 \left[1 - \frac{2}{\pi} \tan^{-1} \frac{|F'|x}{\gamma\sqrt{\mu_0\rho}} \right], \quad (16)$$

which is Equation (12) of Ref. [5].

The growth rate γ is found by requiring the slope of Equation (16) as $x \rightarrow -\infty$ to match Equation (12) as $r \rightarrow r_0$. The result is

$$\gamma = -\frac{\pi}{|F'(r_0)|r_0^3\sqrt{\mu_0\rho}} \int_0^{r_0} g dr, \quad (17)$$

which is $O(\epsilon^2)$, as anticipated. Since $g < 0$, $\gamma > 0$ and the mode is unstable. In light of Equation (8), $\gamma \sim (V_A/L)\epsilon^2$, or $\gamma\tau_A \sim \epsilon^2$. Using Equation (10), the growth rate can be written in terms of the potential energy as

$$\gamma = -\sqrt{\frac{\mu_0}{\rho}} \frac{\delta W_c}{2\pi^2 R \xi_0^2 r_0^3 |F'|}. \quad (18)$$

The system is unstable if $\delta W_c < 0$ for given pressure and current profiles.

I remark here on a peculiarity in this calculation. In the usual formulation of the energy principle (as in Freidberg [10], for example), the growth rate is given by $\gamma^2 = -\delta W/\delta K$, where δK is the kinetic energy functional; thus $\delta W \sim \gamma^2$. However, in this and all subsequent theory of the internal kink and its relation to the sawtooth, $\delta W \sim \gamma$, which implies $K \sim \gamma^{-1}$; see Eq. (18). This relationship can be determined as follows [4].

With time dependence of $e^{\gamma t}$, the kinetic is

$$E_k = \pi\rho R_0\gamma^2 \int_0^a |\Xi|^2 r dr = \pi\rho R_0\gamma^2 \delta K. \quad (19)$$

Here Ξ is the *vector* displacement $\Xi = \xi\hat{e}_r + \xi_\theta\hat{e}_\theta + \xi_z\hat{e}_z$. In the tokamak ordering, $\xi_z \simeq 0$, and using incompressibility with $m = 1$, $\xi_\theta \simeq id(r\xi)/dr$. For the internal kink, the slope of the radial displacement $d\xi/dr$ is very large near the singular radius r_0 ; it is infinite for the ‘‘top hat’’ trial function. The kinetic energy is therefore dominated by ξ_θ^2 in the ‘‘inner’’ layer near the singular surface. Then the integral in Equation (19) is then approximately

$$\delta K \sim \int_0^a |\xi_\theta|^2 r dr \sim \int_0^a \left| i \frac{d\xi}{dr} \right|^2 r^3 dr \sim r_0^3 \int_{-\infty}^{\infty} \left| \frac{d\xi_{in}}{dx} \right|^2 dx. \quad (20)$$

Using $\xi_{in}(x)$ from Equation (16), the last integral is found to be $\sim \gamma^{-1}$, so that $E_k \sim \gamma$ and is consistent with Equation (18).

Some literature [12, 11] defines a non-dimensional growth rate as $\lambda_H = \gamma r_0/V_{A0}$, where

$$V_{A0} = \frac{B_\theta}{\sqrt{\mu_0 \rho}} r_0 \frac{q'(r_0)}{q(r_0)} . \quad (21)$$

Then using Equation (7) and $q(r_0) = 1$, we have

$$\lambda_H = -\frac{\mu_0}{(B_{\theta 0} q'_0 r_0 \xi_0)^2} \frac{\delta W_c}{2\pi R} , \quad (22)$$

which is the equivalent of Equation (II.20) of Ref. [12].

The procedure for finding the growth rate by matching the slope of the inner solution as $x \rightarrow -\infty$ to the slope of the outer solution as $r \rightarrow r_0$ is similar to the method of matched asymptotic expansions[13] that is used in the analysis of resistive instabilities[14]. In that case, a small parameter (e.g., the resistivity) multiplies the highest derivative in the equation, and this term can be ignored everywhere except near the rational surface. The solution is again divided into “inner” and “outer” parts. The lower order differential equation is solved in the outer region, the higher order equation (with rescaled independent variable) in the inner region, and the solutions are asymptotically matched to find the growth rate. The procedure used here is different in that the equation in the outer region, Equation (11) with $\gamma = 0$, is of the same order (in derivative) as the equation in the inner region, Equation (14). A possible justification of this approach is as follows.

We have seen that, away from the rational surface r_0 (i.e., in the outer region), the parameters of the problem scale as $F \sim 1$, $\gamma \sim g \sim \epsilon^2$, and $\xi = \xi_0 + \epsilon^2 \xi_2$ where $\xi_0 \sim 1$ is the trial function given by Equation (9). The term in Equation (11) that is proportional to γ^2 is therefore $\sim \epsilon^4$, and can be ignored compared with F . At $O(\epsilon^2)$, the equation in the outer region is therefore

$$\frac{d}{dr} \left[F^2 r^3 \frac{d\xi_2}{dr} \right] - g\xi_0 = 0 . \quad (23)$$

Integration from 0 to $r < r_0$, where ξ_0 is constant, yields Equation (12), and integration from $r > r_0$ to a , where $\xi_0 = 0$, yields Equation (13).

In the inner region, defined by $F \sim \epsilon^2$, γ^2 and F^2 are of the same order, and both terms must be retained. The term $g\xi_2$ would seem to be the same order ($\sim \epsilon^4$), but becomes $\sim \epsilon^6$ when the rescaled variable $x = (r - r_0)/\epsilon^2$ is introduced. The result is Equation (14). Asymptotic matching of the slopes of the inner and outer solutions produces the growth rate.

The comment that “inertia resolves the singularity” refers to the fact that r_0 is a singular point of Equation (11) when $\rho\gamma^2 = 0$, i.e., $F(r_0) = 0$. When $\rho\gamma^2$ is retained, r_0 reverts to an ordinary point.

3.1.2 Nonlinear Ideal MHD

The rigid shift of the interior of the plasma column that results from the ideal internal kink mode displacement in a cylinder makes it a candidate for the cause of sawtooth oscillations in a tokamak. The relevant question then relates to its nonlinear saturation amplitude. The solution of this problem was reported in Ref.[5]. The result is that the saturation level is too small to account for the experimental observations.

The approach is to find a “neighboring” helical equilibrium that satisfies force balance, has the same magnetic flux as the original cylindrical equilibrium, and matches smoothly with the linear solution given in Section 3.1.1, above. The calculation is complicated and tedious, and only the general approach is outlined here.

Since the displacement for the internal kink mode varies as $\xi(r)e^{i\tau}$, where $\tau = kz + \theta$, we look for equilibrium solutions that are also functions of r and τ ; τ is called the helical coordinate. In addition to force balance, these states must be dynamically “accessible” within the context of ideal MHD. This means that they must have the same values of toroidal and poloidal magnetic flux. It can be directly verified that, in ideal MHD with helical symmetry, the helical flux function $\psi = krA_\theta - A_z$ satisfies $d\psi/dt = \partial\psi/\partial t + \mathbf{V} \cdot \nabla\psi = 0$, so that ψ is a constant of the motion for any fluid element. Further, $\mathbf{B} \cdot \nabla\psi = 0$, so that the equations for the helically distorted flux surfaces are $\psi = \text{constant}$. Since ψ is a constant of the motion of a fluid element, it can be determined by its value $\psi_0(r)$ in the circular, undistorted state. Evaluating the constant at $\theta = 0$, we conclude

$$\psi(r, \theta) = \psi_0(r - \xi) , \quad (24)$$

for all θ . [Here, $\xi = \xi(r, \theta)$] These arguments assume that the displacement of the flux surfaces inside the singular surface is “rigid”. They assume that flux is conserved, and that the neighboring helical state is “accessible”. Further, since near the singular surface $\partial\psi_0/\partial r = Fr$, where $F = \mathbf{k} \cdot \mathbf{B}$, Equation (24) can be expanded in a Taylor series to yield

$$\psi = \psi_0 - \xi r F + \frac{1}{2}\xi^2 (rF)' + \dots . \quad (25)$$

Force balance is expressed as

$$\mathbf{J} \times \mathbf{B} = \nabla p . \quad (26)$$

In the helical state, the magnetic field is given in terms of the helical flux as

$$\mathbf{B} = \frac{\mathbf{e}_\zeta \times \nabla\psi}{\sqrt{1 + k^2 r^2}} , \quad (27)$$

where

$$\nabla\psi = \hat{\mathbf{e}}_r \frac{\partial\psi}{\partial r} + \hat{\mathbf{e}}_\tau \frac{\sqrt{1+k^2r^2}}{r} \frac{\partial\psi}{\partial\tau}, \quad (28)$$

where $\hat{\mathbf{e}}_\tau = (\hat{\mathbf{e}}_\theta + rk\hat{\mathbf{e}}_z)/\sqrt{1+k^2r^2}$ and $\hat{\mathbf{e}}_\zeta = (\hat{\mathbf{e}}_z - rk\hat{\mathbf{e}}_\theta)/\sqrt{1+k^2r^2}$ are ‘‘helical’’ unit vectors, and $\hat{\mathbf{e}}_r$, $\hat{\mathbf{e}}_\theta$, and $\hat{\mathbf{e}}_z$ are the usual cylindrical basis vectors. This formalism can lead to complicated expressions. Instead, we work with the tokamak ordering $B_z/B_\theta \sim kr \sim \epsilon \ll 1$. Then to $O(\epsilon^2)$ the expression for the current density $\mathbf{J} = \nabla \times \mathbf{B}$ reduces to

$$\nabla^2\psi = J_z(\psi), \quad (29)$$

where ∇^2 is the two-dimensional *cylindrical* Laplacian operator, but $\psi(r, \theta)$ is the *helical* flux.

Finally, we must assure that the displacement of the flux surfaces is approximately incompressible. This is accomplished by requiring that the area of the displaced helical flux surface be the same as the area of the corresponding undisplaced circular flux surface, i.e.,

$$\int_{\tau_H} r dr d\theta = \int_{\tau_c} r dr d\theta, \quad (30)$$

where the helical and cylindrical flux surfaces τ_H and τ_c are defined by the flux function ψ .

Equations (29) and (30) form the basis of the theory. The approach will be to find a solution of these nonlinear equations in the vicinity of the singular surface, and then require that these match smoothly to the linear solution in the outer regions. This will yield a value for the displacement amplitude ξ_0 ; see Equation (9).

Now we start the heavy lifting, and we will do as little of it as possible. Within the thin boundary layer surrounding the singular surface, the radial variation of ψ is much faster than the angular variation, and Eq. (29) can be written approximately as $d^2\psi/dr^2 = J(\psi)$. This will be developed into an equation for $r(\psi)$, the position of the helical flux surface with label (value) ψ . Multiplying by $d\psi/dr$, we have

$$\frac{d\psi}{dr} \frac{d^2\psi}{dr^2} = J(\psi) \frac{d\psi}{dr}, \quad (31)$$

or

$$\frac{1}{2} \frac{d}{dr} \left[\left(\frac{d\psi}{dr} \right)^2 \right] = J(\psi) \frac{d\psi}{dr}. \quad (32)$$

Integrating, we have, symbolically,

$$\left(\frac{d\psi}{dr}\right)^2 = F(\psi) + G(\theta) , \quad (33)$$

where $F(\psi) = \int^\psi J(\psi')d\psi'$ is a function of ψ and $G(\theta)$ is an integration function. Both are to be determined. (Do not confuse F with $\mathbf{k} \cdot \mathbf{B}$.) From Equation (33), the equation for $r(\psi)$ is

$$\frac{dr}{d\psi} = \frac{\pm 1}{\sqrt{F(\psi) + G(\theta)}} . \quad (34)$$

The choice of sign will be discussed later.

As in the linear theory, when working within a thin boundary layer it is useful to introduce a new variable x , the radius of the flux surface ψ relative to s , the radius of the singular surface. It is related to the displacement by

$$r - x = \xi . \quad (35)$$

Further, from the form of Equation (25), ψ and x are related by $\psi \sim x^2 s (\mathbf{k} \cdot \mathbf{B})'$, or $d\psi \sim x dx$. We can use this *ansatz* in Eq. (34) to express ξ in terms of x as

$$\frac{\partial \xi(x, \theta)}{\partial x} = \pm \frac{x}{\sqrt{f(x) + g(\theta)}} , \quad (36)$$

where f and g are functions related to F and G , above, and are not to be confused with Equations (3) and (4). (Ref. [5] is quite loose with notation, using f and g for different functions. Unless they really *are* the same functions, which is certainly not clear to me!) The integration for x is given in Ref [5] as

$$\xi(x, \theta) = \int_0^x dx' \left(\frac{x'}{\pm \sqrt{f(x') + g(\theta)}} - 1 \right) + h(\theta) . \quad (37)$$

I don't know why this form was chosen.

Now the incompressibility condition, Equation (30) is applied. The argument is somewhat mysterious, and the entire thing is given in three lines of Ref [5]. Using Equation (37) the result is that

$$\oint \frac{d\theta}{\pm \sqrt{f(x) + g(\theta)}} = \frac{1}{x} , \quad (38)$$

where $\oint d\theta \equiv \int_0^{2\pi} d\theta/2\pi$.

Now we start the asymptotics. (Let the asymptotics begin!) As usual, $x \rightarrow \infty$ implies $r \gg s$ and $x \rightarrow -\infty$ implies $r \ll s$. Further, Equation (38) requires that

we choose the positive sign for $x > 0$ and the negative sign for $x < 0$. According to Ref. [5], “this guarantees that the flux surfaces remain intact”.

The change of sign at the singular surface is important. Since $B_\theta \sim d\psi/dr$, and in light of (the reciprocal of) Equation (34), B_θ must incur a jump at the singular surface $x = 0$, i.e., *a current sheet arises at the singular surface*[5]. This has important implications that will be discussed shortly.

Continuing, we must match the asymptotic forms of Eq. (37) to the linear solutions given by Eqs. (12) and (13). After what appears to be a calculation of Herculean proportions, one arrives at [5]

$$\int_0^\infty df \left\{ \frac{\oint d\theta (f+g)^{-3/2}}{[\oint d\theta (f+g)^{-1/2}]^3} \left[(f+g)^{-1/2} - \oint d\theta (f+g)^{-1/2} \right] \right\} = -\xi_0 \cos \theta . \quad (39)$$

This is the “fundamental integral equation for $g(\theta)$ ” [5]. Wow!

If one makes the scale transformations $g \rightarrow \alpha g$ and $f \rightarrow \alpha f$, one finds $\xi_0 \rightarrow \alpha^{1/2} \xi_0$, so that $g/\xi_0^2 \sim 1$. Further matching to the linear solution yields the additional relation

$$\frac{\oint d\theta g(\theta) \cos \theta}{\xi_0} = - \int_0^s \frac{g_1 dr}{s^3 [(\mathbf{k} \cdot \mathbf{B})'_s]^2} , \quad (40)$$

where now g_1 refers to the function g used in Section 3.1.1. Since $g_1 \sim \epsilon^2$, Equation (40) implies $g/\xi_0 \sim \epsilon^2$. Taken together with our previous result, this implies $\xi_0 \sim \epsilon^2$, i.e., *the saturated amplitude of the ideal internal kink mode is very small*, too small to account for the observed sawtooth oscillations.

Reference [5] states that to “actually solve” Equation (39) “is, of course, an almost impossible task”. *Completely* impossible for most mortals, but apparently only “almost impossible” for Rosenbluth. For, in fact, it is shown in Ref. [5] that Eq. (39) can be derived from a variational principle that can be approximately “solved” for ξ_0 using a trial function for $g(\theta)$. The result is

$$\xi_0 = -13 \int_0^s \frac{g_1 dr}{s^3 [(\mathbf{k} \cdot \mathbf{B})'_s]^2} . \quad (41)$$

Since $g_1 \sim \epsilon^2$, the scaling of the displacement is displayed explicitly. Further, since $\int g_1 dr \sim \delta W < 0$, obtaining the helical solution requires that the cylindrical equilibrium be linearly unstable.

The important point is that the saturated nonlinear helical state of the ideal internal kink mode in a tokamak has insufficient amplitude to account for experimental observations. However, Ref [5] goes on to show that the transition to the

helical state is accompanied by voltage spikes and major radius shifts of the correct sign. So the trends are right even if the magnitude is too small. A possible solution lies in the current sheet that occurs at the singular surface in the non-linear state. Perhaps in the presence of finite resistivity, reconnection or tearing modes can occur that can allow the distortion of the column to continue to finite amplitude. That is the next topic for discussion.

3.1.3 Linear Resistive MHD

We now consider the linear stability of the internal kink mode in cylindrical geometry when electrical resistivity is included, i.e., Ohm's law is

$$\mathbf{E} = -\mathbf{V} \times \mathbf{B} + \eta \mathbf{J} . \quad (42)$$

It is well known that this modification of the ideal equations allows the field to move relative to the fluid, and magnetic reconnection to occur at singular surfaces. This process often occurs in the presence of current sheets of the type associated with the ideal internal kink, and therefore may allow for larger nonlinear distortions of the plasma column. The solution of the problem of the resistive internal kink in a cylinder was first reported by Coppi, et. al., Ref [11], and was reviewed in Ref. [12]. The calculation is tedious but standard (although not simple), and we only report the outline here.

The procedure is based on the method of matched asymptotic expansions [13], and was first used on this type of problem in slab geometry by Furth, Killeen, and Rosenbluth (FKR), Ref. [14]. In ideal MHD the displacement satisfies a second order differential equation [see Eq. 11)]. When finite resistivity is included, the the equation becomes fourth order, with the resistivity multiplying the highest order derivative. Since the growth rate of resistive instabilities is expected to scale as some power of the resistivity, and the resistivity is relatively small (i.e., the resistive diffusion time is much longer than the Alfvén time), the bulk of the plasma is ideal and is almost in equilibrium ($\gamma = 0$), and it is governed by Eq. (23). This is called the “outer equation”. In a small region near the singular surface $r = s$, which is a singular point of Eq. (23), both inertia and resistivity must be included, and the full fourth order equation must be solved. This is called the “inner equation”. For this purpose, the independent variable is rescaled so that it runs from $-\infty$ to $+\infty$. The solution of the inner equation, in the limit $x \rightarrow \pm\infty$, must be matched to the solution of the outer equations as $r \rightarrow s$. In slab geometry, the outer solution behaves as $e^{-\alpha|x|}$ as $|x| \rightarrow \infty$, and the dispersion relation results from matching the logarithmic derivatives of the inner and outer solutions at $r = s$ while assuming that ψ , the perturbed flux, is constant in the inner region. The procedure is similar for the internal kink mode in cylinder, except the limiting forms for the outer solution that must be matched by the inner solution are given

by Eqs. (12) and (13), and one can no longer use the “constant- ψ approximation”. This leads to some complications that do not arise in slab geometry.

For the case of the kink mode in cylindrical geometry, the inner equations are [11, 12]

$$\frac{d^2\xi}{dx^2} = \frac{x}{\lambda^2} \frac{d^2\psi}{dx^2}, \quad (43)$$

and

$$\psi = -\xi x + \frac{\epsilon}{\lambda} \frac{d^2\psi}{dx^2}, \quad (44)$$

where $x = (r - s)/s$, $\psi = iB_{1r}/(F's^2)$, $F' = (dq/dr)B_\theta/s$, $\lambda = \gamma\tau_H$, and $\epsilon = \tau_H/\tau_R \equiv 1/S$ is the inverse of the Lundquist number. The last term on the right hand side of Eq. (44) contains the effects of resistivity. The scaling for which all terms in these equations are comparable is

$$\frac{\psi}{\xi} \sim x \sim \lambda \sim \epsilon^{1/3}. \quad (45)$$

This is called the “resistive ordering”.

Equations (43) and (44) can be combined into a fourth order equation that has four solutions. The physically interesting solutions behave as $d\xi/dx \rightarrow 1/x^2$ as $|x| \rightarrow \infty$. This must match to the solution of the ideal outer equations. From Eq. (12) we have that, as $r \rightarrow s$,

$$\lim_{r \rightarrow s} \frac{d\xi_s}{dr} = s \lim_{x \rightarrow 0} \frac{d\xi_2}{dx} = \frac{\xi_0 \mu_0}{(F'sx)^2} \frac{\delta W_c}{2\pi R}, \quad (46)$$

or

$$\left[\frac{1}{\xi_0} \frac{d\xi}{dx} \right]_{r \rightarrow s} = -\frac{1}{\pi} \frac{\lambda_H}{x^2}. \quad (47)$$

where

$$\lambda_H \equiv -\frac{\pi \mu_0}{s^2 F'^2} \frac{\delta W_c}{2\pi R} \quad (48)$$

is related to the expression in Eq. (22). Equation (47) is the expression that must be matched to the behavior of the inner solution as $x \rightarrow -\infty$.

In slab geometry the inner solution is even about $x = 0$. In cylindrical geometry, the inner solution must be matched to the “top hat” solution in the outer region, i.e., $\xi \rightarrow \xi_0$ as $x \rightarrow -\infty$, and $\xi \rightarrow 0$ as $x \rightarrow \infty$. This is facilitated by writing $\xi = \xi_0/2 + \xi_{odd}$, where $\xi_{odd}(-x) = -\xi_{odd}(x)$. We then require that the inner solution satisfy

$$\frac{x^2}{2} \frac{d}{dx} \ln \xi_{odd} = -\frac{\lambda_H}{\pi} \quad (49)$$

for $x/\lambda \rightarrow -\infty$ as $\xi_{odd} \rightarrow \xi_0/2$.

We further introduce the even function [11]

$$\chi(x) = x \frac{d\psi}{dx} - \psi = \lambda^2 \frac{d\xi}{dx} + \chi_\infty, \quad (50)$$

where χ_∞ is a constant. We use these to express ξ and ψ in terms of the new variable χ . The second equality of Eq. (50) gives immediately

$$\xi = -\frac{1}{\lambda^2} \int_x^\infty dx' (\chi - \chi_\infty). \quad (51)$$

The first equality is a differential equation for ψ , $d\psi/dx - \psi/x = \chi/x^2$, which has an integrating factor $1/x$. Then $d/dx(\psi/x) = \chi/x^2$, and integrating from x to ∞ yields the solution

$$\frac{\psi}{x} = -\int_x^\infty \frac{\chi(x')}{x'^2} dx'. \quad (52)$$

The desired expression [11] is found by integrating the right hand side by parts. The result is

$$\psi = -\chi - x \int_x^\infty \frac{d\chi}{dx'} \frac{dx'}{x'}. \quad (53)$$

Now comes some hand waving. From Eqs. (43) and (44),

$$\xi = -\frac{\psi}{x} - \frac{\epsilon\lambda}{x} \frac{d^2\xi}{dx^2}. \quad (54)$$

Then using Eq. (52),

$$\frac{1}{2}\xi_0 + \xi_{odd} = \int_x^\infty \frac{d\chi}{dx'} \frac{dx'}{x'} + \frac{\chi}{x} - \epsilon\lambda \frac{1}{x} \frac{d^2\xi_{odd}}{dx^2}. \quad (55)$$

We now take the limit as $x \rightarrow 0$. First, $\xi_{odd}(0) = 0$. Then, one could possibly argue that $\lim_{x \rightarrow 0} (1/x) d^2\xi/dx^2 = d^3\xi_{odd}/dx^3 \sim O(\epsilon) \ll 1$, which can be ignored. However, I cannot find an argument to ignore $\lim_{x \rightarrow 0} \chi/x$, which seems to diverge. [See Eq. (50).] In any case, there must be some argument to this effect, because a crucial equation of Ref [11] is

$$\xi_0 \simeq 2 \int_0^\infty \frac{d\chi}{dx} \frac{dx}{x}. \quad (56)$$

(I am very interested in learning the origin of this equation.) Further, when $x \rightarrow \infty$, from the first of Eq. (50), $d\psi/dx \simeq \chi/x$, and from Eq. (44), $\psi \simeq -\xi x$. Then, as $x \rightarrow \infty$,

$$\frac{d\xi}{dx} \rightarrow -\frac{\chi_\infty}{x^2}. \quad (57)$$

We can then use Eqs. (56) and (57) in Eq. (49) to yield the condition

$$\chi_\infty = \frac{2\lambda_H}{\pi} \int_0^\infty \frac{d\chi}{dx} \frac{dx}{x}. \quad (58)$$

The plan is now as follows. Substitute the *ansatz* of Eq. (50) into Eqs. (43) and (44). This will yield a second order inhomogeneous differential equation for $\chi(x)/\chi_\infty$, with parameters λ and ϵ . Solve this equation to give $\chi(x; \lambda, \epsilon)/\chi_\infty$. Then the integral on the right hand side of Eq. (58) will be a function of λ and ϵ , multiplied by χ_∞ , which cancels. Equation (58) is then the dispersion relation; in principle it can be solved for the growth rate λ in terms of the resistivity ϵ and the ideal MHD growth rate λ_H . Now we just have to do it!

The second order differential equation for χ is

$$\epsilon\lambda \left(\frac{d^2\chi}{dx^2} - \frac{2}{x} \frac{d\chi}{dx} \right) - (x^2 + \lambda^2) \chi = -x^2 \chi_\infty. \quad (59)$$

Introducing $\hat{x} \equiv x/\delta$, where $\delta^4 = \epsilon\lambda$, and defining $\hat{\lambda} = \lambda/\epsilon^{1/3}$, we have

$$\frac{d^2\chi}{d\hat{x}^2} - \frac{2}{\hat{x}} \frac{d\chi}{d\hat{x}} - (\hat{x}^2 + \hat{\lambda}^{3/2}) \chi = -\hat{x}^2 \chi_\infty. \quad (60)$$

Equation (60) can be solved by expanding in Laguerre polynomials and using many of their mathematical properties[12, Appendix A]. The result is

$$\frac{\chi}{\chi_\infty} = 1 - 2^{-5/2} \hat{\lambda}^{3/2} \int_0^1 dy y^{(\hat{\lambda}^{3/2}-5)/4} (1+y)^{1/2} \exp \left[-\frac{\hat{x}^2}{2} \left(\frac{1+y}{1-y} \right) \right]. \quad (61)$$

That this is a solution can be verified by direct substitution into Eq. (60).

We now substitute Eq. (61) into the matching condition, Eq. (56). The result is

$$1 = \frac{2\lambda_H}{\pi\delta} \int_0^\infty d\hat{x} \frac{\hat{\lambda}^{3/2}}{2^{5/2}} \int_0^1 dy F(y) \alpha(y) e^{-\alpha\hat{x}^2/2}, \quad (62)$$

where $F(y) = y^{(\hat{\lambda}^{3/2}-5)/4} (1+y)^{1/2}$, and $\alpha(y) = (1-y)/(1+y)$. Exchanging the order of integration, and noting $\int_0^\infty e^{-\alpha\hat{x}^2/2} d\hat{x} = \sqrt{\pi/2\alpha}$, we have

$$1 = \frac{\lambda_H \hat{\lambda}^{3/2}}{4\delta\sqrt{\pi}} \int_0^1 dy y^{(\hat{\lambda}^{3/2}-5)/4} (1-y)^{1/2} . \quad (63)$$

This integral can be evaluated with the help of the Beta function (Ref.[15, Section 6.2]; see also Ref.[16, pp. 467 ff], and Ref.[17, pp. 254 ff]), which is defined as

$$B(p, q) = \int_0^1 dy y^{p-1} (1-y)^{q-1} = \frac{\Gamma(p)\Gamma(q)}{\Gamma(p+q)} , \quad (64)$$

where $\Gamma(z)$ is the Euler gamma function. Here we have $p = (\hat{\lambda}^{3/2} - 1)/4$, $q = 3/2$, and $\Gamma(3/2) = \sqrt{\pi}/2$. Using all the definitions of the non-dimensional variables, the final result is the dispersion relation[11, 12]

$$\hat{\lambda} = \hat{\lambda}_H \left[\frac{\hat{\lambda}^{9/4} \Gamma((\hat{\lambda}^{3/2} - 1)/4)}{8 \Gamma((\hat{\lambda}^{3/2} + 5)/4)} \right] , \quad (65)$$

where $\hat{\lambda}_H = \lambda_H/\epsilon^{1/3}$.

For finite $\hat{\lambda}$, marginal ideal stability, $\hat{\lambda}_H = 0$, requires $\Gamma((\hat{\lambda}^{3/2} - 1)/4) \rightarrow \infty$, or $\hat{\lambda}^{3/2} = 1$. This corresponds to $\lambda = \epsilon^{1/3}$, or $\gamma_{\tau_H} = S^{-1/3}$. This is the resistive internal kink growth rate. For $\epsilon \rightarrow 0$, ($S \rightarrow \infty$), we have $\hat{\lambda} \ll 1$. In that case it is easy to show that the large amplitude expression for the Gamma-functions [15, 6.1.39] yields the expression $\delta W_c - i\omega/\omega_A = 0$ [see Eq. (48)], which is the ideal kink dispersion relation. We also note that, for $0 < \hat{\lambda} \ll 1$, we have approximately

$$\hat{\lambda} \simeq \left[\frac{1}{\hat{\lambda}_H} \frac{\Gamma(\frac{5}{4})}{\Gamma(-\frac{1}{4})} \right]^{4/5} , \quad (66)$$

which, since $\Gamma(-1/4) = -\pi/(4\Gamma(1/4) \sin \pi/4) < 0$, can be positive even when $\hat{\lambda}_H$ is negative; the resistive kink can be unstable even when the ideal kink is stable. This is sometimes called the ‘‘reconnecting mode’’[12]. We will see in Section 3.2.1 that toroidal effects can stabilize the ideal internal kink mode. Therefore, the reconnecting mode is a candidate for sawtooth oscillations in a tokamak.

In light of Eq. (22), Eq. (65) can be written as

$$\delta W_c + 8S^{-1/3} \hat{\lambda}^{-5/4} \frac{\Gamma((\hat{\lambda}^{3/2} + 5)/4)}{\Gamma((\hat{\lambda}^{3/2} - 1)/4)} = 0 , \quad (67)$$

where some constants have been absorbed into δW_c . This is a form of the dispersion relation that we will see again.

3.1.4 Extended MHD Effects

In extended MHD, Ohm's law is written as

$$\mathbf{E} = -\mathbf{V} \times \mathbf{B} + \eta \mathbf{J} + \frac{1}{ne} [\mathbf{J} \times \mathbf{B} - \nabla p_e] , \quad (68)$$

where p_e is the electron pressure. Since $\mathbf{V} \simeq \mathbf{V}_i$ and $\mathbf{J} = ne(\mathbf{V}_i - \mathbf{V}_e)$, Eq. (68) can be written as

$$\mathbf{E} = -\mathbf{V}_e \times \mathbf{B} - \frac{1}{ne} \nabla p_e + \eta \mathbf{J} , \quad (69)$$

which is the inertialess electron equation of motion (i.e., with $m_e = 0$). Extended MHD is thus a model in which electrons and ions are treated as separate fluids, with (in this case) neglect of the electron mass. They introduce the effects of separate ion and electron drifts. These are sometimes called “kinetic effects”, although kinetic theory is not involved. We can use the (center of mass) equation of motion to rewrite Eq. (68) as

$$\mathbf{E} = -\mathbf{V} \times \mathbf{B} + \eta \mathbf{J} + \frac{m_i}{e} \frac{d\mathbf{V}}{dt} + \frac{1}{ne} \nabla p_i , \quad (70)$$

where the total pressure is $p = p_i + p_e$.

In ideal MHD, the dispersion relation can be written symbolically as $\omega^2 + \gamma_{MHD}^2 = 0$, where the time dependence is $e^{i\omega t}$, and γ_{MHD} is the ideal MHD growth rate, related to δW as described in Section 3.1.1. In the analysis using extended MHD, the term $d\mathbf{V}/dt$ in Equation (70) introduces a factor of $i\omega$ that does not occur in ideal MHD. It is well known that this modifies the dispersion relation to be of the form $\omega(\omega - \omega_*) + \gamma_{MHD}^2 = 0$, where $\omega_* = \mathbf{B} \times \nabla p_i / (neB^2)$ is the ion drift frequency. The frequency ω becomes complex. It is not surprising that the extended MHD modifications to the resistive internal kink mode appear in a similar fashion.

Since we expect the growth rate to remain small compared with the Alfvén frequency, the plasma away from the singular surface remains governed by ideal MHD and is in quasi-equilibrium. Modifications to the dispersion relation all arise from the inner layer.

The analysis[12] is similar to that of Section 3.1.3. In dimensionless form, the inner layer equations are

$$\lambda(\lambda - i\lambda_i) = x\psi'' , \quad (71)$$

$$\psi = -x\xi + \frac{\epsilon}{\lambda - i\lambda_e} \psi'' . \quad (72)$$

Here, $\lambda = -i\omega\tau_H$, $\lambda_{e,i} = -\omega_{*e,i}$, $\psi = iB_{r1}/(rdF/dr)_s$, $\epsilon = 1/S$, prime denotes differentiation with respect to $x = (r - s)/s$, and all quantities are evaluated at

the singular surface $r = s$. The solutions of these equations must be matched to the ideal MHD outer solution. The matching condition remains Eq. (56).

Again introducing the *ansatz* [see Eq. (50)]

$$\chi(x) = x\psi' - \psi = \lambda(\lambda - i\lambda_i)\xi' + \chi_\infty, \quad (73)$$

we find [12] that χ satisfies the differential equation

$$\frac{d^2\chi}{d\hat{x}^2} - \frac{2}{\hat{x}}\frac{d\chi}{d\hat{x}} - (\hat{x}^2 + \Lambda^{3/2})\chi = -\hat{x}^2\chi_\infty, \quad (74)$$

where $\hat{x} = x/\delta$, $\delta^4 = \epsilon\lambda(\lambda - i\lambda_i)/(\lambda - i\lambda_e)$, $\Lambda = [\hat{\lambda}(\hat{\lambda} - i\hat{\lambda}_e)(\hat{\lambda} - i\hat{\lambda}_i)]^{1/3}$, $\hat{\lambda} = \lambda/\epsilon^{1/3}$, and $\hat{\lambda}_{e,i} = \lambda_{e,i}/\epsilon^{1/3}$. Equation (74) is identical in form to Eq. (60), and the ensuing analysis proceeds exactly as in Section 3.1.3. The result is the dispersion relation

$$\left[\hat{\lambda}(\hat{\lambda} - i\hat{\lambda}_i)\right]^{1/2} = \frac{\hat{\lambda}_H}{8}\Lambda^{9/4}\frac{\Gamma((\Lambda^{3/2} - 1)/4)}{\Gamma((\Lambda^{3/2} + 5)/4)}. \quad (75)$$

Note that when $\lambda_{e,i} = 0$, Eq. (75) reduces to Eq. (65).

3.1.5 The Ion-kinetic Regime

The extended MHD model of Section 3.1.4 accounts for the effects of finite ion skin depth ($d_i/L > 0$). (If gyro-viscosity and ion diamagnetic heat flux are included, lowest order corrections in $k_\perp\rho_i$ are also captured.) It remains a fluid model. However, for some JET discharges, and for expected ITER parameters, the ion gyro-radius is expected to be larger than the width of the resistive layer about the rational surface $r = r_1$ (the subscript referring to the $m = 1$ mode). While the fluid model (in fact, equilibrium ideal MHD) remains valid in the outer region, the ions in the inner layer must now be treated with kinetic theory. The ordering of length scales $\rho_i > \delta_\eta > d_e$, where $\rho_i = V_{thi}/\Omega_{ci}$ is the ion gyro-radius, $\delta_\eta = s_1^{-1/3}S^{-1/3}r_1$ is the resistive layer width, $s_1 = r_1q'(r_1)$ is the ‘‘shear parameter’’, and $d_e = c/\omega_{pe}$ is the electron inertial skin depth, is called the *ion kinetic regime*. The width of the singular layer is now set by the ion gyro-radius.

The analysis of this regime is reported in Refs. [18] and [19]. Within the inner layer the electrons are treated as a fluid, while the ion dynamics are described by the Vlasov equation. These papers present the most involved and complex asymptotic gymnastics that I have ever seen, and I certainly cannot follow it in any detail. They use a ballooning formalism applied to low- m and $-n$ modes (e.g., $m = 1$, $n = 1$), which they claim to justify on the basis of the thinness of the inner layer. This allows the use of Fourier (or ‘‘Fourier-like’’, my quotes) transforms in the radial direction, and results in a second order differential equation for the perturbed current density as a function of z , the transform variable conjugate to

the radial coordinate; z has units of L^{-1} . As usual, the dispersion relation result from matching the solution of this inner equation to the ideal MHD solution in the outer region. (The inner solution involves combinations of the ever-popular confluent hypergeometric function.) For later reference, we give the approximate dispersion relation in the large ion gyro-radius regime [Eq. (15) of Ref. [19]]:

$$z_A \lambda_H = \frac{\pi}{2} \left(\frac{g z_\rho^2}{\mu z_A^2} \right)^{1/2}, \quad (76)$$

where $g = 1 - i\lambda_*/\lambda$, $\lambda = -i\omega\tau_H$, $\lambda_* = -\omega_*\tau_H$, $\mu = (1 + \tau)/(\tau + i\lambda_*/\lambda)$, $\tau = T_e/T_i$, $\lambda_i = -\lambda_*(1 + \eta_i)/\tau$, $\eta_i = d \ln T_i / d \ln n$, $z_A^2 = 1/[\lambda(\lambda - i\lambda_i)]$, $z_\rho^2 = \lambda/[\tau\rho_i^2(\lambda - i\lambda_i)]$, and λ_H is given by Eq. (48). Of course, this is to be solved for the growth rate λ . [Several remarks are in order. First, the more accurate version of the dispersion relation (Eq. (11) of Ref. [19]) involves 14 gamma-functions, so Eq. (76) is an improvement. Second, I suspect the factor of $\pi/2$ is a better approximation of 1 than the solution of Eq. (76) is of the actual growth rate. Finally, while Eq. (76) appears to be relatively simple, I am reminded of Feynman's caution regarding simplifying notation [20]: First, write down in a long column all the known laws of physics; say there are N of them. Then, move everything to the left hand side, so that only zeros appear on the right. Then define a vector A of length N that contains all the left hand sides as its elements. The laws of physics are now expressed in the elegant and compact form $A = 0$, which is simultaneously accurate and completely devoid of content. Nonetheless, we will have occasion to refer back to Eq. (76) in Section 4.2.]

3.1.6 Nonlinear Evolution

The work of RDR (Ref. [5]; see Section 3.1.2, above) showed that the ideal internal kink mode saturates with a low amplitude. The work of Coppi, et. al., Ref. [11], suggested that, in the presence of resistivity, the mode may continue to grow to finite amplitude due to magnetic reconnection. Kadomtsev [6] speculated, but did not prove, that the reconnection may continue until the magnetic island at the rational surface expels the original magnetic axis from the plasma, thus rendering $q(0) > 1$ and stabilizing the plasma.

Kadomtsev envisioned a sequence of events that begin with $q(0) > 1$. As the core of the plasma heats (Ohmically or otherwise) the current density becomes more peaked on axis, driving $q(0)$ lower, eventually becoming less than unity. This occurs on a relatively slow time scale governed by the heating rate. Then the $q = 1$ singular surface appears in the plasma, and the resistive internal kink is destabilized. As the nonlinear evolution expels the original magnetic axis, the $q = 1$ singular surface disappears, and $q(0)$ is restored to greater than unity. This

process occurs on a faster time scale governed by the dynamics of the nonlinear resistive kink. The process can then repeat, leading to a series of relaxation oscillations with slow “rise time” and fast “crash time”, as observed during sawtooth oscillations in experiments.

Obtaining the full nonlinear evolution of the internal kink mode in a cylinder requires numerical solution of the resistive (or extended) MHD equations. For the resistive equations, this was first reported by Waddell, et. al. [21], and Sykes and Wesson [22]. Of necessity, these calculations were limited to relatively low S (high resistivity). (No value of S is cited by Sykes and Wesson [22], but the grid was reported as $14 \times 14 \times 10!$ It is unfortunate that the online archive of Nuclear Fusion do not go back as far as 1976, so I do not have access to Ref. [21].) The time evolution of the helical flux surfaces during the nonlinear evolution of the internal kink mode, taken from Ref. [22], is shown in Fig. 4. Note the expulsion of the original magnetic axis by the magnetic island, confirming Kadomtsev’s intuitive picture [6]. The calculation even produced sawtooth-like relaxation oscillations, as shown in Fig. 5. This demonstrates the potential power of even coarse computational models to reveal important nonlinear dynamics.

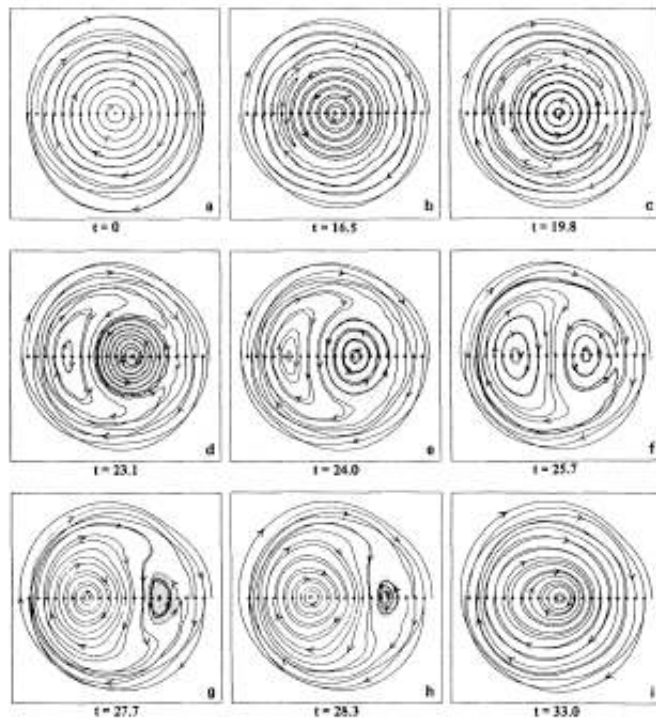


Figure 4: Evolution of the helical flux surfaces during the nonlinear evolution of the resistive internal kink mode [22].

These results, even at relatively large S , have been confirmed by many numerical simulations over the ensuing decades. The problem with these results is that the reconnection rate (a measure of the time for the sawtooth crash phase) is longer than is observed in experiments.

In the higher temperature, nearly collisionless regimes, as may be expected in modern tokamaks, the extended MHD model of Section 3.1.4 must be employed. A “reduced” version of extended MHD is contained in the so-called four-field model [23], which is in the spirit of reduced MHD but contains FLR and two-fluid (drift) effects. Aydemir [24] applied this model to the nonlinear evolution of the $m = 1$ mode in a cylinder. For $S \simeq 10^6$, the internal kink mode was found to have an accelerated growth rate in the nonlinear regime that was large enough to possibly account for the experimentally observed fast sawtooth crash time.

The evolution of the helical flux surfaces for this case, taken from Ref. [24], is shown in Fig. 6. The fast reconnection is due to two-fluid effects. The decoupling of the ions and electrons in the inner layer leads to the formation of a Y-point instead of an X-point, as is usual in resistive MHD. This allows the fluid to evacuate the reconnection region more efficiently, resulting in an enhanced reconnection rate. This is illustrated in Fig. 7 [24], which shows the evolution from an X-point to a Y-point later in the nonlinear evolution.

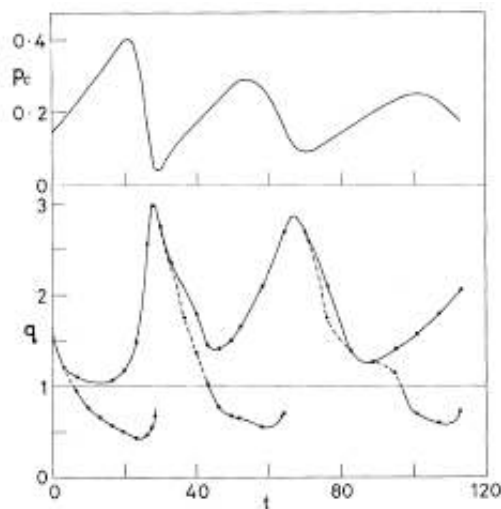


Figure 5: Sawtooth-like relaxation oscillations in the on-axis values of the pressure (top) and q (bottom) during the nonlinear evolution of the internal kink mode [22].

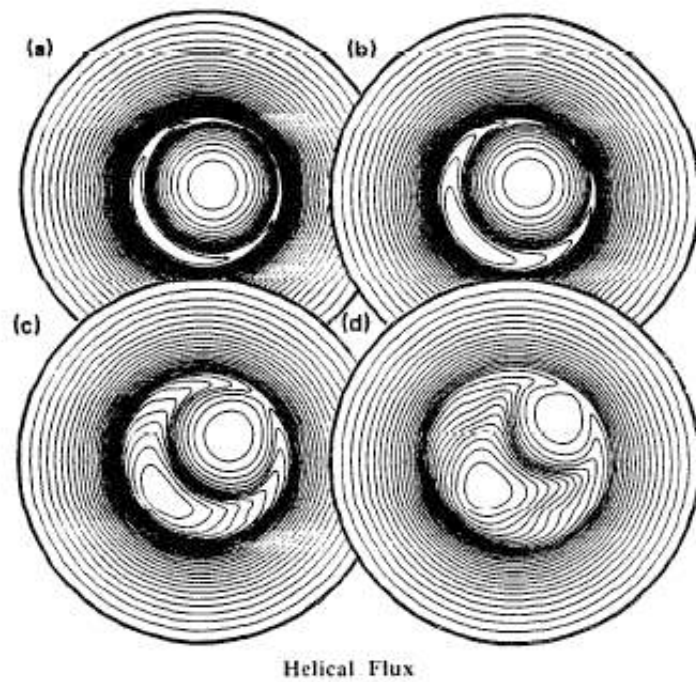


Figure 6: Evolution of the helical flux surfaces during the nonlinear evolution of the resistive internal kink mode using the “four-field model” (extended MHD) [23, 24].

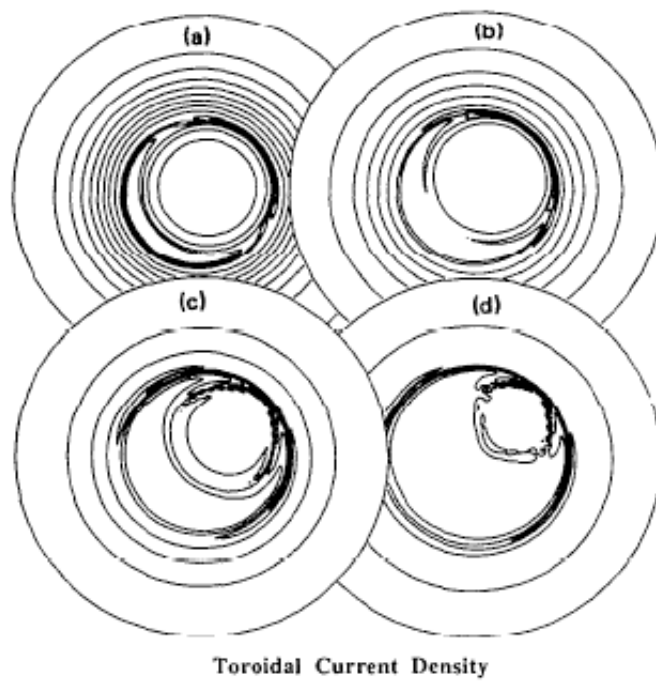


Figure 7: Evolution of the toroidal current density during the nonlinear evolution of the resistive internal kink mode using the “four-field model” (extended MHD) [23, 24].

3.2 Toroidal Geometry

Linear theory and nonlinear numerical simulation in cylindrical geometry indicate that the resistive internal kink, suitably modified with two-fluid and FLR effects as might occur in a high temperature tokamak, remains a viable candidate for sawtooth oscillations. However, it is well known that the toroidal, as opposed to cylindrical, geometry of a tokamak plays an important role in determining the plasma dynamics. Two effects are primary. The first is that the magnetic well induced by the toroidal geometry can cause the almost collisionless particles to be become trapped on the outboard side of the torus. This leads to non-Maxwellian velocity distributions and modifications of the moment equations that describe the fluid plasma. The second is that the poloidal mode number m is no longer a good “quantum number”; the toroidal geometry induces a coupling between all the m -numbers for a given n . Since the $m = 2, n = 1$ ideal mode is stable in a straight system [10, p. 420], one expects the overall effect to be stabilizing for the $m = 1$ internal kink mode.

We will deal with both of these effects in the following sections. We take the second effect first.

3.2.1 Linear Ideal MHD

The analytic modifications to the linear ideal MHD stability analysis of the internal kink (the $m = 1, n = 1$ mode) in circular cross section toroidal geometry were reported by Bussac, et al. [25], and summarized by Freidberg [10, pp. 419ff]. They recognized that, for low toroidal mode n , the toroidal correction to the cylindrical potential energy, Eq. (10), due to poloidal mode coupling is $O(\epsilon^2)$ (here $\epsilon = s/R$ is the aspect ratio of the singular surface), which is the the same order as δW_c itself. In particular, after “a rather involved calculation that is too complicated to reproduce here” [10, p. 419], they found the ideal MHD δW in toroidal geometry to be

$$\frac{\delta W}{W_0} = \left(1 - \frac{1}{n^2}\right) \delta \tilde{W}_c + \frac{1}{n^2} \delta \tilde{W}_T, \quad (77)$$

where $\delta \tilde{W}_c$ is the normalized cylindrical δW (i.e., the integral in Eq. (10)), $\delta \tilde{W}_T$ is the toroidal correction, and W_0 contains all the normalization constants. When $n \rightarrow \infty$, the cylindrical results apply. However, the stability properties of the $n = 1$ internal kink mode are strongly affected.

The toroidal correction $\delta \tilde{W}_T$ is in general a complicated expression [25]. However, for the case of a parabolic current profile, with $|q_0 - 1| \ll 1$ and $q_0 < 1$, one finds

$$\delta\hat{W}_T \sim \frac{3n^2 s^4}{R_0^2} (1 - q_0) \left(\frac{13}{144} - \beta_p^2 \right) , \quad (78)$$

where

$$\beta_p = -\frac{R_0^2}{n^2 s^2} \int_0^s r^2 \beta' dr , \quad (79)$$

is the “poloidal beta” inside the singular surface, and $\beta' = 2\mu_0 r^2 p' / (R_0^2 q^2 B_\theta^2)$ is the normalized pressure gradient [10, p. 413]. Note that, when $n = 1$, the cylindrical contribution to δW vanishes (see Eq. (77)), and stability is given by Eq. (78). Therefore, in a torus (of circular cross section), the internal kink mode is ideal MHD stable in the limit $\beta_p \rightarrow 0$. Instability requires $\beta_p > \sqrt{13}/12 \sim 0.3$. Thus, the statement is often made that, in a torus, the internal kink is pressure driven rather than current driven.

Of course, the preceding analysis has been based on circular cross section toroidal geometry, and Eqs. (78) and (79) were derived for a parabolic current profile. In the latter case there is strong shear, and therefore strong coupling between the $m = 1$ and $m = 2$ contributions, leading to stabilization. We might expect that weaker shear might lead to weaker coupling, and therefore weaker stabilization. This and other generalizations of the analysis require a numerical solution of the ideal equations. These calculations [26, 27, 28, 29] confirm the general trend toward stabilization in toroidal geometry. However, for profiles with very low shear, the stabilization disappears and $q_0 > 1$ is required regardless of β_p [10, p. 420].

The toroidal stabilization of the ideal internal kink was anticipated in Section 3.1.3, Eq. (66), where it was shown that the resistive kink can be unstable even when the ideal kink is stable. This is the case in toroidal geometry. However, note from Eq. (66) that the magnitude of resistive growth rate can be a relatively strong function of the ideal growth rate (even if the latter is negative).

3.2.2 Trapped Particles

The orbits of individual charged particles can be quite complicated in a toroidal plasma. Of course, their most rapid motion consists of spiraling about the magnetic field. This gyro-motion can be “averaged out” of the equations of motion, and the resulting “gyro-averaged” dynamical model refers to the motion of the particle’s “guiding center”. The motion of these centers is governed by a set of Hamiltonian equations, which, in addition to the usual constants of the motion, admit several further quantities that are “almost” conserved if the conditions seen by the moving particle vary only slowly. These are called adiabatic invariants [30, 31, 32]. These

play an important role in determining the motion of the guiding centers in a toroidal plasma.

In a torus, the equilibrium magnetic field strength is a function of the major radius R , with the field larger on the inboard side than the outboard side. Because of the adiabatic invariants, if the collision frequency is sufficiently low, some charged particles can become trapped in this magnetic well, and “bounce” between the mirror points of the magnetic field with frequency ω_b . The trapping of particles depends primarily on their kinetic energy parallel to the magnetic field; particles with lower parallel energy can become trapped. In addition to the bounce motion, the guiding centers also experience several slow “drift” motions that cause them to move off a given magnetic field line. One of these, given in the large aspect ratio approximation as [30, p. 131]

$$\mathbf{v}_d = -\frac{v^2 + v_{\parallel}^2}{2\Omega_{\phi}R} \hat{\mathbf{z}}, \quad (80)$$

where $\Omega_{\phi} = ZeB_{\phi}/m_i$ is the ion cyclotron frequency, is in the vertical direction and causes the orbits of the trapped particles to trace out banana-like trajectories when projected on the poloidal plane; this region of parameter space is called the “banana regime”. Another drift effect causes the banana orbits not to close exactly upon themselves, but rather drift slowly in the toroidal direction. Again at large aspect ratio, this *precessional frequency* ω_p is given approximately by [30, p. 145]

$$\omega_p \tau_b \simeq \frac{q\epsilon^{1/2}\rho_{\theta}}{r} \ll 1, \quad (81)$$

where $\epsilon = r/R$ is the inverse aspect ratio, $\rho_{\theta} = V_{thi}/\Omega_{\theta}$ is the ion Larmor radius calculated with the poloidal field B_{θ} , and $\tau_b \equiv 1/\omega_b$ is the bounce frequency of the banana orbit [30, p. 132]. Of course, all of these concepts have a rigorous basis in Hamiltonian dynamics [30, 31, 32].

We (I) surmise that the drift given by Eq. (80) does not survive so-called “bounce averaging”, i.e., averaging over time long compared with the bounce time. However, the drift given by Eq. (81) represent a secular increase in the toroidal location of the center of the banana orbit, i.e., $\phi(t) = \phi_0 + \omega_p(t - t_0)$, so that it survives bounce averaging. It is this drift, sometimes called just the “magnetic drift”, that is important in the theory of trapped particle modification of the internal kink mode.

The presence of these trapped particles alters the plasma distribution function, and hence the specific form of the fluid equations that determine the dynamics of the bulk of the plasma (specifically, the pressure tensor of the fluid equations is modified). Global plasma stability can be affected.

For our purposes, trapped particles can be classified as “energetic” or “thermal”. Energetic trapped particles have a distribution function that is distinct from

the bulk of the plasma. They may arise from the injection of a mono-energetic beam of ions, or (optimistically) as α -particles resulting from fusion reactions. Their distribution function is strongly non-Maxwellian, and are sometimes considered as a distinct plasma “species” (electrons, ions, energetic ions). In contrast, thermal trapped particles represent the high energy tail of the bulk (Maxwellian) plasma. (Technically speaking, once these particles become trapped they no longer have a Maxwellian distribution. So, what is really meant is the fraction of the particles making up the “core” fluid that become trapped. ($\sim \epsilon^{1/2}$)) In Section 3.2.3 we will deal with the effects of thermal trapped particles on MHD stability. Effects due to energetic trapped particles will be discussed Section 3.2.4 and following.

3.2.3 Thermal Trapped Particles

When the plasma is collisional (i.e., the collision frequency is the fastest “microscopic” frequency), the distribution function becomes a “local” Maxwellian, i.e., a Gaussian distribution with a different characteristic temperature, density, and velocity at each point in space. In this case, MHD theory is well justified and the well-known energy principle [33, 10] can be applied to determine stability. (We remark that MHD is often useful even when this assumption is not valid [10].) However, the theory should be revisited when the distribution function deviates from Maxwellian, for example in the case of thermal trapped particles.

This was first done in 1958 by Kruskal and Oberman [34]. They derived an energy principle for a plasma with a general distribution function, and established several theorems relating to necessary and sufficient conditions for stability. They derived an expression for the potential energy $\delta W = \delta W_D + I$ (in their notation), where δW_D is the hydrodynamic potential energy for the case of an *anisotropic* pressure [33] and I is a complicated expression containing velocity space integrals of the distribution function. They showed that I is positive, so that $\delta W \leq \delta W_D$, i.e., if the plasma is stable with the particle (kinetic) theory, it is stable under (anisotropic) fluid theory. However, for the case of *isotropic* pressure, $\delta W \geq \delta W_H$ (where δW_H is the “hydrodynamic” potential energy), i.e., hydrodynamic stability implies kinetic stability for isotropic pressure.

The paper is typical of its era: terse, complicated, with just little enough information to be understandable only by experts who already know the result. (There is also an interesting footnote and acknowledgement suggesting that Rosenbluth may have arrived at the same result independently.) For our purposes, the paper itself is almost worthless, other than to recognize that trapped thermal particles can alter the potential energy, and hence the picture of MHD stability. In later work [35, 36], their contribution is summarized as $\delta W = \delta W_{MHD} + \delta W_{KO}$, where δW_{KO} (for “Kruskal-Oberman”) represents the contribution from the thermal trapped particles, i.e., the complicated integral over velocity space. Ref. [36] gives the

terse expression

$$\delta\hat{W}_{KO} = 0.6 \frac{c_p \epsilon_1^{1/2} \beta_{i0}}{s_1}, \quad (82)$$

where $\delta\hat{W}$ is a normalized potential energy, c_p is an integral depending on the pressure profile, ϵ_1 is the aspect ratio at the $q = 1$ surface ($\epsilon_1^{1/2}$ is the fraction of trapped particles within this surface), β_{i0} is the peak ion toroidal beta, and s_1 is the “shear parameter” at the $q = 1$ surface: $s_1 = r_1 q'(r_1)$. The origin of this expression, and its relationship to the contents of Ref. [34], elude me. (According to Ref [46], it is “... obtained analytically from integrating the trapped thermal ion distribution over the zeroth-order model displacement obtained by Bussac, et al., in the limit $\epsilon \rightarrow 0$.”) With regard to stability, “... the trapped thermal particles contribute to both δW_{MHD} and $\delta W_{trapped}$ ” (δW_{KO} ?). “Their contribution to δW_{MHD} is destabilizing but is nearly cancelled by their contribution to $\delta W_{trapped}$. The net result appears to be stabilizing since only the circulating particles, which experience predominantly favorable curvature contribute to the potential energy.” [35] If you say so!

3.2.4 Energetic Trapped Particles: Ideal Fishbones

The early theoretical work on the effect of trapped energetic particles on plasma stability indicated that they were stabilizing for ballooning modes, but that they might also be associated with recently observed “fishbones” oscillations [37]. Large scale sawtooth-like oscillations were reported on the PDX experiment, with growth rate consistent with the internal kink mode. Additional high frequency oscillations were associated with the sawteeth during neutral beam injection; see Fig. 8 [38]. The real frequency of these oscillations was approximately the precession rate of the injected particles [see Eq. (81)]. The magnetic signals were primarily $m = 1, n = 1$, with a significant $m = 2$ component. These “fishbone” oscillations were accompanied by losses of energetic beam particles, which degraded the efficiency of neutral beam heating. It was speculated [38] that these losses “could have serious consequence for neutral beam and other auxiliary heating methods” in fusion reactors. This unstable activity is a result of a resonant interaction between some aspect of the orbital motion (likely the precessional motion) of the energetic particles of the beam and the MHD properties of the bulk plasma.

The velocity distribution function $f(v)$ (or, equivalently, $F(E)$, where $E = m_i v^2/2$ is the particle energy) for the bulk plasma is locally a Maxwellian, i.e., a Gaussian distribution characterized at each point in space by local values of temperature, density, and mean flow velocity. In contrast, energetic particles generally begin their lives with a single value of energy E_0 , so that, when they

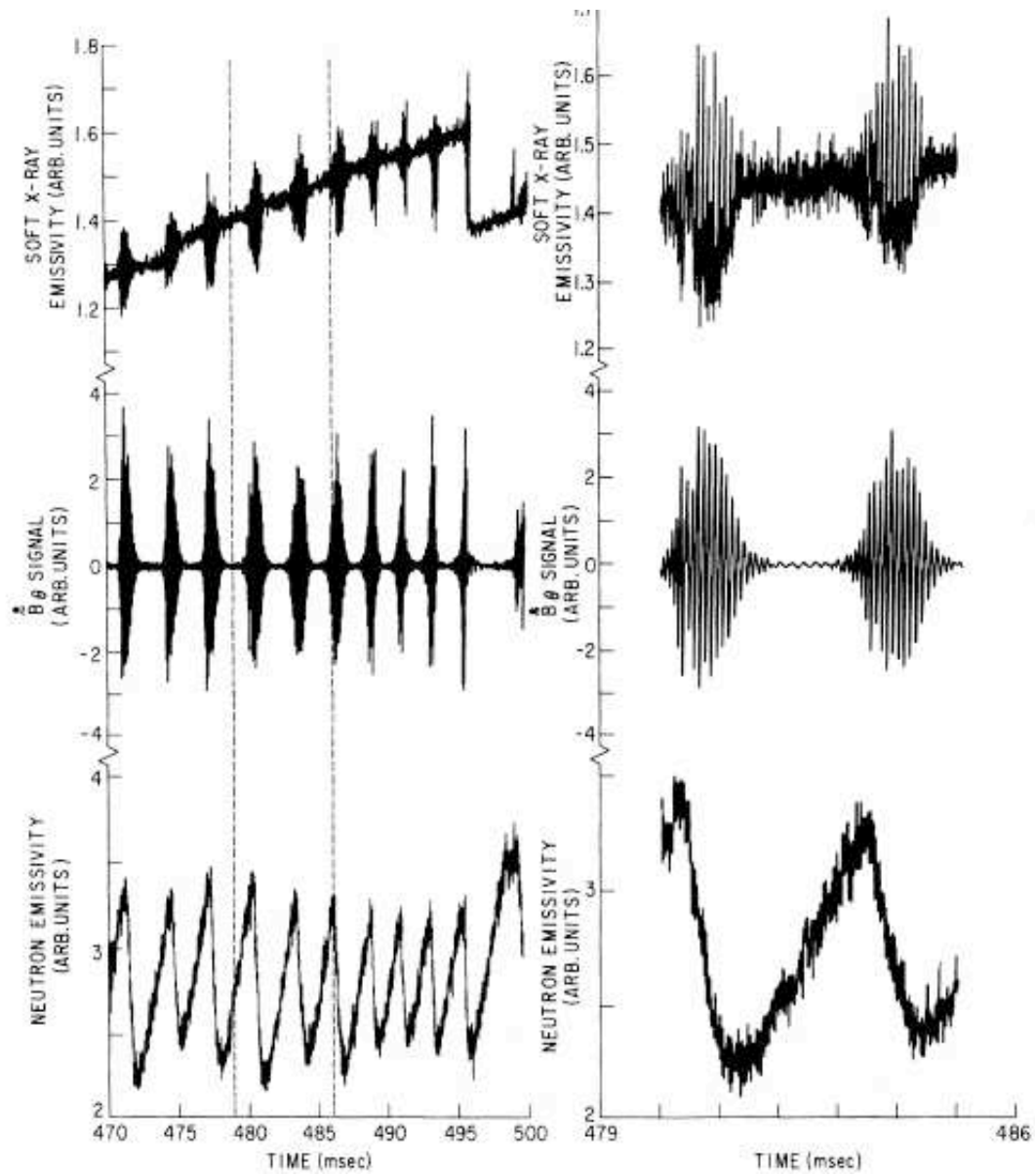


Figure 8: “Fishbone” oscillations associated with sawteeth as measured in the PDX tokamak [38].

first appear, their distribution function is $f(E; t = 0) \simeq \delta(E - E_0)$. (The initial energy E_0 may be the energy of the beam ions, or, in the case of fusion from D-T reactions, α -particles with $E_0 = 3.5$ MeV.) In any case, these ions are generally faster than the background (bulk) Maxwellian ions, but slower than the electrons, i.e., $V_{th_i} \ll v_E \ll V_{th_e}$, where V_{th_s} is the thermal speed for species s , and $v_E = \sqrt{2E_0/m_E}$ is the initial velocity of the energetic ions (see Ref. [30, pp. 35ff] for a thorough discussion). They subsequently undergo collisions with the background ions and electrons, and their distribution function is modified.

For the parameter regime just described, the initial “slowing down” of the energetic species is due to collisions with the electrons. As they lose energy and get slower, they eventually begin to interact with the bulk ions. This occurs at a critical speed v_C corresponding to an energy of approximately $m_E v_C^2/2 \simeq [m_E/(m_i^{2/3} m_e^{1/3})]T_e$, where T_e is the electron temperature. For α -particles, this energy is approximately $50 T_e$. Above v_C , the energetic ions are slowed by the electrons, but are not significantly deflected (like a bowling ball moving through ping pong balls). Below v_C , collisions with ions cause deflection to become comparable to drag (as when the bowling ball begins to interact with other bowling balls). This information can be used to define a collision operator for this process [30]. If energetic particles are born isotropically with velocity v_E at a rate S per unit volume, the resulting kinetic equation for the energetic particle distribution function is

$$\frac{\partial f_E}{\partial t} = \frac{1}{v^2 \tau_S} \frac{\partial}{\partial v} \left[(v^3 + v_C^3) f_E(v) \right] + \frac{S \delta(v - v_E)}{4\pi v_E^2}, \quad (83)$$

where τ_S is the “slowing-down time”, defined in Ref. [30, p. 40]. In steady state, the solution is

$$f_E(v) = f_S \equiv \frac{S \tau_S}{4\pi(v^3 + v_C^3)}, \quad (84)$$

for $v < v_E$, and 0 for $v > v_E$. Equation (84) is called (creatively!) the “slowing-down distribution”.

The fluid equations for each species s in the plasma are derived from successive velocity moments of the species’ plasma kinetic equation $df_s/dt = C(f)$ [30, 32], where C contains the effects of collisions. The MHD and extended MHD equations are appropriate combinations of these moment equations [32]. It is not surprising, then, that the presence of a non-Maxwellian species, such as energetic ions, can alter the form of the fluid equations. The calculation of these modifications is daunting in general, and is no less so in the case of a single energetic (or *hot*) ion species [39]; the calculation is extremely complicated and only the results are given here.

The modification to the fluid equations appears additively in the form the divergence of a pressure tensor in the equation of motion. For species s , the pressure tensor is defined as

$$\mathbf{P}_s \equiv \int d^3v f_s m_s (\mathbf{v} - \mathbf{V}_s) (\mathbf{v} - \mathbf{V}_s) , \quad (85)$$

where \mathbf{V}_s is the mean (fluid) velocity, and f_s the distribution function, of species s . For our case, $s \rightarrow h$, the hot (energetic) ion species. The linearized perturbation of the hot ion pressure tensor can be written in terms of the displacement as [39]

$$\delta \mathbf{P}_h = -\xi \cdot \nabla \cdot \left[P_\perp \mathbf{I} + (P_\parallel - P_\perp) \hat{\mathbf{b}} \hat{\mathbf{b}} \right]_h + \delta \hat{P}_\perp \mathbf{I} + (\delta \hat{P}_\parallel - \delta \hat{P}_\perp) \hat{\mathbf{b}} \hat{\mathbf{b}} , \quad (86)$$

where P_\perp and P_\parallel refer to the (CGL) perpendicular and parallel (to \mathbf{B}) pressures, and $\hat{\mathbf{b}}$ is a unit vector in the direction of \mathbf{B} . The perturbed pressures are to be calculated from moments of the perturbed distribution function for the hot particle species.

The plasma displacement ξ will also affect the evolution of the hot particle distribution function. The calculation of P_\parallel and P_\perp for the hot particle species requires solving for the perturbed distribution function δf_h from the linearized kinetic equation. Since the unperturbed orbits of the energetic particles are the mathematical characteristics of the collisionless linearized kinetic equation, the parameters that characterize these orbits appear in the solution. The analytic solution is further enabled by again assuming large aspect ratio, i.e, $\epsilon = a/R \ll 1$, along with the ordering $\beta_{pc} \sim O(1)$, $\beta_{ph} \sim O(\epsilon)$, $T_c/T_h \sim O(\epsilon^2)$, and $n_h/n_c \sim O(\epsilon^3)$, where the subscripts c and h stand for core (bulk) and hot (energetic) species, respectively. Additionally, for PDX, $|\omega/\omega_A| \sim |\bar{\omega}_{dh}/\omega_A| \sim O(\epsilon^2)$, where $\omega \sim \gamma$ is the internal kink growth rate, ω_A is the Alfvén frequency, $\bar{\omega}_{dh}$ is the hot particle precession frequency [see Eq. (81)], and $\omega_d \sim v_d/a$ is the “magnetic drift frequency” [see Eq. 80]. Under these assumptions the gyro-kinetic approximation can be used. The result is (in CGS units) [39]

$$\delta f_h = \frac{e}{m} \left[\delta \phi \frac{\partial}{\partial E} - \frac{\mu}{\omega_c} \frac{\delta B_\parallel}{c} \frac{\partial}{\partial \mu} \right] f_{0h} + \delta H_h , \quad (87)$$

where f_{0h} is the equilibrium hot particle distribution function, and δH_h satisfies

$$\left[v_\parallel \frac{\partial}{\partial l} - i(\omega - \omega_{dh}) \right] \delta H_h = i \frac{e}{m} Q \delta \psi , \quad (88)$$

with $E = v^2/2$, $\mu = v_\perp^2/2B$, ω_c is the cyclotron frequency, $\partial/\partial l \equiv \hat{\mathbf{b}} \cdot \nabla$, $\delta \psi = \delta \phi - v_\parallel \delta A_\parallel / c + v_\perp^2 \delta B_\parallel / 2\omega_c c$, $Q \equiv (\omega \partial/\partial E + \hat{\omega}_{*h}) f_{0h}$, $\hat{\omega}_{*h} \equiv -(i/\omega_c) \hat{\mathbf{b}} \times \nabla \ln f_{0h}$, $\omega_{dh} \equiv -i \mathbf{v}_d \cdot \nabla$, and \mathbf{v}_d is the “magnetic drift velocity” [see Eq. (80)]. Note

that Q , $\hat{\omega}_{*h}$, and ω_{dh} are differential operators, so that Eqs. (87) and (88) are quite complicated. The perturbed scalar and vector potentials are related to the displacement ξ by Ohm's law, $c\nabla\delta\phi = -i\omega\xi \times \mathbf{B}$, and the Lorentz gauge condition $\omega\delta A_{\parallel}/c = -i\partial\delta\phi/\partial t$.

As noted, Eqs. (87) and (88) are formidable. However, “when one notes that the frequencies are much smaller than the hot particle transit and bounce frequencies, Eq. (88) can be solved readily for both trapped (t) and untrapped (u) particles” [39]. The resulting expressions can be used to evaluate the trapped particle contributions to the perturbed pressure tensor. The result is Eq. (86), with

$$\delta\hat{P}_{\perp} = 2^{7/2}\pi m_h B \int_{B_{max}^{-1}}^{B^{-1}} d\alpha (1 - \alpha B)^{1/2} \int_0^{\infty} dE \frac{E^{5/2} Q}{\omega - \bar{\omega}_{dh}} \bar{J} \frac{\alpha B}{2(1 - \alpha B)}, \quad (89)$$

and

$$\delta\hat{P}_{\parallel} = 2^{7/2}\pi m_h B \int_{B_{max}^{-1}}^{B^{-1}} d\alpha (1 - \alpha B)^{1/2} \int_0^{\infty} dE \frac{E^{5/2} Q}{\omega - \bar{\omega}_{dh}} \bar{J}, \quad (90)$$

where $\alpha = \mu/E = v_{\parallel}^2/(v^2 B)$,

$$J = \frac{1}{2}\alpha B \nabla \cdot \xi_{\perp} - \left(1 - \frac{3}{2}\alpha B\right) \xi_{\perp} \cdot \kappa, \quad (91)$$

κ is the field line curvature, and $\bar{A} \equiv (\oint A dl/|v_{\parallel}|)/(\oint dl/|v_{\parallel}|)$ denotes the bounce average. The integral over α is an integral over the region accessible by the energetic trapped particles, $1/B_{max}$ is the “turning point” (or mirror point) of the bounce orbit. Note that Eqs. (89) and (90) contain resonant denominators, so we may expect some “activity” associated with $\omega \sim \bar{\omega}_{dh}$, the bounce average toroidal precession frequency of the energetic trapped particles.

Sorting through all of the above complexity, it can be seen that the resulting expression for $\nabla \cdot \mathbf{P}$ is linearly proportional to the displacement ξ , so that the presence of energetic particles results in an additive term to the ideal MHD dispersion relation. Doting this with ξ^* and integrating yields the energy principle $\delta W_{MHD} + \delta W_k + \delta I = 0$, where δI is the inertial term (only important in the inner singular layer), and the energetic particle contribution can be written as [39]

$$\delta W_k = -2^{9/2}\pi^3 m_h \int R B r dr \int_{B_{max}^{-1}}^{B^{-1}} d\alpha \int_0^{\infty} dE E^{5/2} K_b \bar{J}^* \frac{Q}{\omega - \bar{\omega}_{dh}} \bar{J}, \quad (92)$$

where $(*)$ denotes the complex conjugate, $K_b \equiv \oint (d\theta/2\pi)(1 - \alpha B)^{-1/2}$, and δW_{MHD} is the toroidally modified MHD potential energy; see Eq. (77). (The ξ -dependence enters through J .) We note the possibilities that the presence of energetic particles

may destabilize ($\delta W < 0$) a system that is ideal MHD stable ($\delta W_{MHD} > 0, \delta W_k < 0$), or vice versa.

For PDX parameters, the dispersion relation for the $m = 1, n = 1$ internal kink mode can be written approximately as [39]

$$-i\frac{\omega}{\tilde{\omega}_A} + \delta\hat{W}_f + \delta\hat{W}_k = 0, \quad (93)$$

where $\tilde{\omega}_A = V_A/(3^{1/2}Rsq'_s)$, $\delta\hat{W}_f$ is given approximately by Eq. (78), and

$$\begin{aligned} \frac{\delta W_k}{2\pi R} &\simeq \pi^2 m_h 2^{3/2} \frac{|\xi_{r0}|^2}{R^2} \int_0^s r dr \int_{1-r/R}^{1+r/R} d(\alpha B) \int_0^\infty dE E^{5/2} \frac{K_2^2}{K_b} \left[\frac{Q}{\tilde{\omega}_{dh} - \omega} \right]_{1,1} \\ &\equiv |\xi_{r0}|^2 \left(\frac{sB_0}{2R} \right)^2 \delta\hat{W}_k \end{aligned} \quad (94)$$

where $K_2 = \oint (d\theta/2\pi) \cos\theta (1-\alpha B)^{-1/2}$, and $B \simeq B_0(1-r \cos\theta/R)$. “By substituting into $\delta\hat{W}_k$ a monoenergetic, single magnetic moment distribution F_{0h} we find a thresholdless [sic] unstable solution with $\omega_r \simeq \tilde{\omega}_{dh}$ and ω_i increasing with $\langle\beta_{ht}\rangle$ (the average trapped particle β within the $q = 1$ surface), with $\omega_{*h}/\tilde{\omega}_{dh} > 0$.” [39]. The primary physics is identified as “coupling between a negative-energy/dissipation trapped-particle precession mode and a core-plasma MHD mode, which is positively dissipated because of the $\omega_r \sim k_{\parallel}V_A$ resonance” [39].

So, as I read it so far, with PDX parameters and a “delta-function” hot particle distribution function, there is always an unstable mode (it is “thresholdless”). The mode has a real frequency ω_r that is on the order of the bounce averaged hot particle “magnetic drift frequency” $\tilde{\omega}_{dh} \sim v_d/r$ [see Eq. (80), and the discussion following Eq. (88); it is clear from later context that ω_{dh} refers to the precessional drift frequency]. This real frequency is also $\sim k_{\parallel}V_A$, so that there is strong coupling to the MHD branch, which gives it an “internal-kink-like” character.

For a slowing-down distribution $f_{0h} = cE^{-3/2}\delta(\alpha - \alpha_0)$ for $E < E_m$, see Eq. (84), with a single magnetic moment α_0 , the dispersion relation is

$$-i\Omega \frac{\tilde{\omega}_{dm}}{\tilde{\omega}_A} + \delta\hat{W}_{fc} + \langle\beta_{ht}\hat{I}_0\rangle\Omega \ln\left(1 - \frac{1}{\Omega}\right) = 0, \quad (95)$$

where $\Omega = \omega/\tilde{\omega}_{dm}$, $\langle y \rangle \equiv (2/s^2) \int_0^s yr dr$ is an average inside the singular surface, $\delta\hat{W}_{fc}$ corresponds to the contribution to $\delta\hat{W}_f$ from the core plasma inside the singular surface, the subscript m refers to evaluation at $E = E_m$, and \hat{I}_0 is a complicated expression involving complete elliptic integrals. This equation can be solved for (complex) Ω with $\langle\beta_{ht}\hat{I}_0\rangle$ and $\delta\hat{W}_{fc}$ as parameters. A “simple analysis” [39] of Eq. (95) reveals that the internal kink mode is destabilized if β_{ht} exceeds a certain value, even if $\delta\hat{W}_{fc} > 0$, i.e., if the discharge is ideal MHD stable. The

critical value is $\langle \beta_{ht} \hat{I}_0 \rangle_{crit} = \bar{\omega}_{dm} / \pi \bar{\omega}_A$. The growth rate is peaked near $\delta \hat{W}_{fc} \simeq 0$, and drops sharply as $\delta \hat{W}_{fc}$ increases (becomes more MHD stable). “This may account for the predominance of fishbones near marginal [MHD] stability” [39]. With some further approximations, the growth rate can be written approximately as [39]

$$\omega_i \simeq \frac{\pi^2}{4} \tilde{\omega}_A \left[\langle \beta_{ht} \hat{I}_0 \rangle - \langle \beta_{ht} \hat{I}_0 \rangle_{crit} \right] . \quad (96)$$

The analysis of Chen, et al. [39] is terse and complicated. I have not been able to follow it step-by-step, as in (for the most part) MHD. I have only tried to parrot the important points, the most important of which is that the interaction between energetic trapped particles and MHD can lead to significant modifications of the stability properties of a toroidal plasma (in particular, a tokamak). For the present parameters (i.e., PDX) the result is destabilizing; ideally stable plasmas become unstable, and new overstable modes (fishbones) appear near the marginal ideal MHD point. We will see that, in different parameter regimes, the result can be stabilization of otherwise unstable MHD configurations.

As an interesting aside, the form of Eq. (96) suggests a simple low-dimensional non-linear model that reproduces many of the characteristics of fishbones [39]. Equation (96) suggests that the amplitude of the magnetic perturbation of the mode satisfies an equation of the form

$$\frac{dA}{dt} = A \Gamma (\beta_h - \beta_{crit}) , \quad (97)$$

with $\Gamma = \tilde{\omega}_A (\pi^2/4) \langle \hat{I}_0 \rangle$, and β_h is the hot particle β within the $q = 1$ surface. We expect β_h to change due to energetic particle loss across the $q = 1$ surface, i.e., *beam loss* induced by the $m = 1, n = 1$ perturbation. If one assumes that this loss occurs on a time scale much shorter than the beam deposition time, and that the rate of particle loss is approximately constant until a significant fraction of the particles have been lost, then we can surmise that β_h may be governed by an equation of the form

$$\frac{d\beta_h}{dt} = D - AZ \beta_{max} \theta (\beta_h - \beta_{min}) , \quad (98)$$

where D is the net deposition rate of trapped particles within the $q = 1$ surface, Z is a measure of the particle loss rate, and $\theta(x)$ is a Heaviside function that introduces the nonlinearity into the model. (Chen, et. al. [39] note that $m = 2$ perturbations, which arise from the toroidal coupling, extend to the plasma boundary, and are observed in the experiment, are necessary for complete loss of the beam particles.) The real frequency of the mode is given by $\omega_r \simeq \bar{\omega}_{dh}$; see the discussion in the paragraphs following Eq. (94). (I remark that, in their

results, Ref. [39] continually refers to $\bar{\omega}_{dh}$ as the “toroidal precession frequency”, whereas in their preliminary discussion this quantity is called the “magnetic drift frequency”.)

The simultaneous solution of Eqs. (97) and (98) with $\omega_r = \bar{\omega}_{dh}$ is shown in Fig. 9 for parameters similar to PDX. Note the similarity to the observed fishbones, shown in Fig. 8. This is quite a synthesis!

3.2.5 Energetic Trapped Particles: Resistive Effects on Fishbones

The effects of resistivity can be included by adding the hot particle contribution, $\delta\hat{W}_k$, to the resistive dispersion relation, Eq. (67), and replacing δW_{MHD} with its toroidal version. This was first done by Biglari and Chen [40]. The resulting dispersion relation can be written schematically as

$$\delta\hat{W}_c + \left\langle \frac{\omega}{\bar{\omega}_{dh} - \omega} \frac{\hat{\omega}_{*h}}{\hat{\omega}_{dh}} \beta_{ht} \right\rangle = -8S^{-1/3} \Omega^{-5/4} \frac{\Gamma \left[\left(\Omega^{3/2} + 5 \right) / 4 \right]}{\Gamma \left[\left(\Omega^{3/2} - 1 \right) / 4 \right]}, \quad (99)$$

where $\delta\hat{W}_c$ is the “normalized version of the usual core plasma ideal MHD potential energy” [40], $\Omega = -iS^{-1/3}\omega/\omega_A$, and $\langle \dots \rangle$ denotes velocity space average over the trapped region. Ref. [40] is clear and unambiguous that $\bar{\omega}_{dh}$ is the “energy dependent, bounce-averaged precessional drift frequency”; modes “become destabilized when the wave structure starts to resonate with the precessional drift of the hot particle banana centers ($\omega \simeq \omega_{dh}$)” [40]. A detailed calculation [40] shows that, in the presence of resistivity, the value critical of β_{ht} for the onset of fishbones is modified to $\langle \beta_{ht} I_0 \rangle_{crit}^{resistive} \sim (\omega_r / |\bar{\omega}_{dm}|)^{9/4} \langle \beta_{ht} I_0 \rangle_{crit}^{ideal}$, where $\langle \beta_{ht} \hat{I}_0 \rangle_{crit}^{ideal} = \bar{\omega}_{dm} / \pi \bar{\omega}_A$ [see

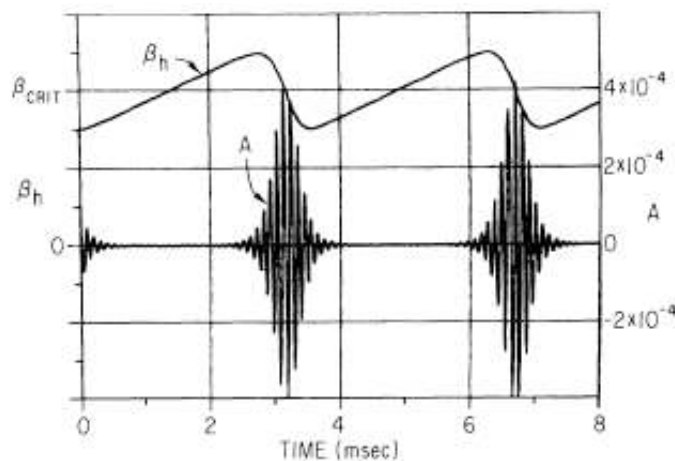


Figure 9: Fishbone oscillations from the solution of Eqs. (97) and (98) for PDX parameters.[39].

discussion following Eq. (96)]. This is valid for $\bar{\omega}_{dm}/\omega_R < 1$ (here $\omega_R = S^{-1/3}\omega_A$ is the “resistive interchange frequency”). Above this value the ideal results hold. The dependence of the critical β on the precessional frequency is shown in Fig. 10 [40].

The primary physical conclusion is that “the resistive correction to the ideal dispersion relation affects the growth rate only as an effective $\delta\hat{W}$ and this contribution is a stabilizing one. Physically, the instability mechanism has the character of a negative-energy/dissipation trapped particle precession mode in the ideal region which becomes positively dissipated in the inertial layer. The inclusion of resistivity acts to enhance this sink mechanism so that it becomes harder to drive the instability” [40]. In this case, resistivity is stabilizing. Further, for JET parameters $\bar{\omega}_{dm}/\omega_R \sim 10^{-2} \ll 1$, so the ideal theory would indicate that JET should be “virulently unstable” [40] to fishbones (see Fig. 10). However, because of resistivity, the threshold for the onset of fishbones “is actually raised by dissipation to such an extent that it becomes prohibitive for these ‘resistive fishbones’ to assert themselves” [40].

3.2.6 Energetic Trapped Particles: Sawteeth

The stabilization of the fishbones at high- S (high temperature and strong magnetic field) was encouraging, and the observation of long sawtooth-free periods

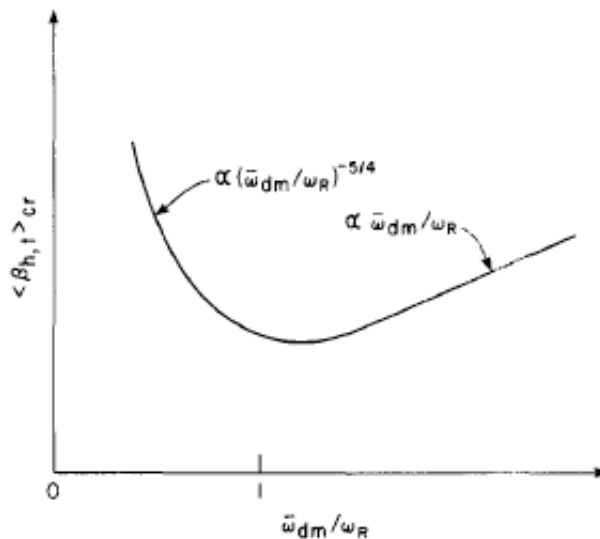


Figure 10: Critical hot particle β for the onset of fishbones using resistive theory [40].

on JET [41] during minority ion heating was suggestive of a stabilization mechanism for the resistive internal kink mode. This was first investigated by White, Rutherford, Colestock and Bussac [42], who found that "the presence of a high-energy trapped particle population introduces a stabilization of the sawtooth in a tokamak". However, they cautioned that, while "the stabilization of the sawtooth mode in low- β discharges is encouraging, at higher β the same ... population should destabilize the fishbone branch ... [which] should then be expected to limit the trapped-particle population to a value too low to provide sawtooth stabilization" [42].

Ref. [42] presents both numerical and analytic results. The numerical results use δW_k of Ref. [39] and the extended MHD inner layer modifications as shown in Eq. (75), while the analytic results neglect these " ω_* " effects, as "they have the effect of decreasing the growth rate and giving the mode a real frequency; but they complicate the algebra, and the qualitative behavior of the solution can be understood without them" [42]. So, while the analytic results include toroidal ideal MHD, resistive inner layer physics, and energetic trapped particle physics, they ignore 2-fluid effects. We will only discuss the analytic results here.

Neglecting 2-fluid effects, the dispersion relation is [42]

$$\delta W_c + \delta W_k + 8S^{-1/3}\Omega^{-5/4}\frac{\Gamma[(\Omega^{3/2} + 5)/4]}{\Gamma[(\Omega^{3/2} - 1)/4]} = 0, \quad (100)$$

where, as usual, $\Omega = -i\omega/\omega_R$, $\omega_R = S^{-1/3}\omega_A$, and $\omega_A = V_A/\sqrt{3}Rsq'$, and all expressions are evaluated at the singular surface $r = s$ where $q(s) = 1$. The energetic particle contribution is expressed as

$$\delta W_k = \frac{2^{3/2}}{B^2}m\pi^2 \left[\int d(\alpha B) \int \frac{dE E^{5/2} K_2^2 \left(\omega \frac{\partial}{\partial E} + \hat{\omega}_* \right) F_{0h}}{K_b(\omega_d - \omega)} \right], \quad (101)$$

where, again as before, $[y] \equiv (2 \int_0^s y r dr) / s^2$, $\alpha = v_\perp^2 / v^2$, K_2 and K_b are "elliptic integrals arising from bounce averaging", and $\hat{\omega}_*$ is "a differential operator associated with the drift frequency" [42]. The dependence only on the region inside the singular surface is because of the use of the cylindrical internal kink trial function, Eq. (9), which vanishes for $r > s$. In a torus, of course, there will be higher- m components that will introduce dependence on the entire plasma radius.

We are interested in the hot particle effects on the resistive kink mode. Therefore, in light of the discussion following Eq. (65), we set $\delta W_c = 0$. Specific stability predictions depend on the choice of the hot particle equilibrium distribution function, F_{0h} . For the case of the slowing-down distribution [see Eq. (84)]

$$F_{0h}(E, \mu) = n(r) E^{-3/2} \delta(\mu/E - \alpha_0), \quad E < E_m, \quad (102)$$

where E is the energy, μ is the magnetic moment, and $dn/dr \sim 1/\epsilon$, one finds [42]

$$\delta W_k = i \frac{\beta_h}{\epsilon} \Omega A \ln \left(1 + \frac{i}{A\Omega} \right), \quad (103)$$

[see Eq. (95)] where β_h is the trapped hot-particle β , and $A = \omega_R/\omega_{dm}$, the ratio of the resistive growth rate to the maximum toroidal precession frequency, which is given (for deeply trapped particles) by (approximately)

$$\omega_{dm} = \frac{E_m q}{mr R \omega_c}, \quad (104)$$

where ω_c is the cyclotron frequency of the energetic ions. The dispersion relation for the resistive internal kink is therefore [42]

$$8 \frac{\Gamma \left[\left(\Omega^{3/2} + 5 \right) / 4 \right]}{\Gamma \left[\left(\Omega^{3/2} - 1 \right) / 4 \right]} + i \frac{\beta_h}{\epsilon} S^{1/3} \Omega^{9/4} A \ln \left(1 + \frac{i}{A\Omega} \right) = 0. \quad (105)$$

According to Eq. (105), trapped particles only become important when $(\beta_h/\epsilon)S^{1/3}A = (\beta_h/\epsilon)\omega_A/\omega_{dm} > 1$ (this statement is not entirely clear to me), independent of S . This is within a factor of π of the fishbone threshold [see the discussion following Eq. (95)]. Note that (using Eq. (104) with $E = nT$, and recalling that ω_A refers to the background plasma and not the hot particles) this quantity is proportional to the hot trapped particle density n_h and magnitude of the charge, and is independent of its mass and energy.

Two limits are of interest. The first occurs for small $\beta_h A S^{1/3}$, which corresponds to the onset at small β_h . This suggests expanding Eq. (105) about $\Omega = 1$, which is the solution for $\beta_h = 0$. Using $\Gamma(3/2) = \sqrt{\pi}/2$ [15, 6.1.9] and $1/\Gamma(3\delta/8) \simeq 3\delta/8$, with $\delta \ll 1$ [15, 6.1.3], we find

$$\Omega \simeq 1 - 2iA \frac{\beta_h}{\epsilon} \frac{S^{1/3}}{3\sqrt{\pi}} \ln \left(1 + \frac{i}{A} \right). \quad (106)$$

For very energetic particles (consistent with the initial assumption that $T_h/T_c \sim 1/\epsilon^2$), $A \ll 1$, $\ln(1 + i/A) \simeq i\pi/2 - \ln A$, so that the imaginary part of ω increases and the growth rate increases. The effect becomes more pronounced for $A \simeq 1$, i.e., when the precession of the energetic particles resonates with the resistive frequency ω_R [42]. Therefore, at small β_h (really $\beta_h \omega_A/\omega_{dm}$) energetic particles become destabilizing to the resistive internal kink.

The second limit is (not surprisingly!) $\beta_h S^{1/3} A \gg 1$. In that case there are two roots: $\Omega \rightarrow \infty$ and $\Omega \rightarrow 0$. The first root yields a mode that is “strongly stabilized” [42]. The second root is given asymptotically as $\Omega = (\beta_h/\epsilon)S^{1/3}$. “As long as $\langle \omega_d \rangle > \omega_R$,” (brackets undefined) “the first root ... is the tearing-mode root,

and [the second] describes the fishbone. If instead $\langle \omega_d \rangle < \omega_R$, the trapped particles destabilize the tearing mode and its asymptotic limit is given by [the second root]” [42]. That is, for the case of very energetic particles and “large enough” β_h , there is a stabilizing effect on the sawtooth, and the stabilization increases with β_h . However, at larger β_h the fishbone becomes destabilized. Although it is not obvious, according to Ref [42] “... to stabilize the tearing mode it is necessary to produce a trapped particle density which is large enough to destabilize the fishbone”.

This is very dense stuff. The conclusion [42] is that “... the presence of a high-energy trapped ion population introduces a stabilization of the sawtooth in a tokamak. ... at higher β the same ... population should destabilize the fishbone branch ... The fishbone should then be expected to limit the trapped-particle population to a value too low to provide sawtooth stabilization.”

4 Consolidation

4.1 General Stability in a Torus

The results of Section 3.2.6 indicated that, within the context of trapped-particle modified resistive MHD, complete stabilization of the sawtooth may be difficult or impossible to achieve. The problem is that, in order to stabilize the resistive internal kink mode, the hot particle β must be so high as to destabilize the fishbone. A more complete analysis of the problem was first briefly reported by White, Bussac and Romanelli [43], and later in much more detail by White, Romanelli and Bussac [44].

There are two primary differences with the previous analysis [42]. The first is the inclusion of extended MHD effects (see Section 3.1.4). The second is accounting for the possibility that δW_c , the ideal MHD potential energy, may not vanish. (Recall that in Ref. [42], $\delta W_c = 0$.) Indeed, an important and seemingly contradictory conclusion of Refs. [43] and [44] is that complete stabilization of the sawtooth (resistive internal kink mode) with energetic particles requires that $\delta W_c < 0$, i.e., that the *ideal* internal kink be *unstable*. The analysis is thorough and complex, and includes many limiting and special cases. We will only summarize a few of the basic results here.

The dispersion relation, including ideal MHD, resistive MHD, extended MHD, and energetic particle effects is the consolidation of the results of the previous sections. In the notation of Ref. [44],

$$-\frac{\gamma_I}{\omega_A} + \delta W_k - \frac{8i\Gamma \left[(\Lambda^{3/2} + 5) / 4 \right] [\omega (\omega - \omega_{*i})]^{1/2}}{\Lambda^{9/4} \Gamma [(\Lambda^{3/2} - 1) / 4] \omega_A} = 0 , \quad (107)$$

where $\Lambda = -i[\omega(\omega - \hat{\omega}_{*e})(\omega - \omega_{*i})]^{1/3}/\gamma_R$, $\gamma_R = S^{-1/3}\omega_A$, $\omega_{*i} = -(c/neBr)dP_i/dr$, $\omega_{*e} = (c/neBR)dP_e/dr$, $\hat{\omega}_{*e} = \omega_{*e} + 0.71(c/eBr)dT_e/dr$, δW_k is given by Eq. (101), and $\gamma_I \equiv -\omega_A \delta W_c$ is the ideal MHD growth rate in a torus, given by Eq. (78). Note that, in this analysis, γ_I is treated as a parameter. The dispersion relation depends on the energetic trapped particle equilibrium distribution function, F_{0h} , and the six frequencies ω_A , ω_d , ω_{*i} , $\hat{\omega}_{*e}$, γ_I , and γ_R . Ref. [44] examines many of these combinations. We will only look at a few.

We first examine the case of the slowing-down distribution in the ideal limit. Then $\delta W_k = (\beta_h/\epsilon)(\omega/\omega_{dm}) \ln(1 - \omega_{dm}/\omega)$. Taking $\gamma_R \rightarrow 0$, the dispersion relation is [44]

$$-\frac{\gamma_I}{\omega_A} - i \frac{[\omega(\omega - \omega_{*i})]^{1/2}}{\omega_A} + \frac{\beta_h}{\epsilon} \frac{\omega}{\omega_{dm}} \ln\left(1 - \frac{\omega_{dm}}{\omega}\right) = 0. \quad (108)$$

The threshold condition for instability is that ω be real. Making this assumption along with the condition $\omega < \omega_{dm}$, and taking the real and imaginary parts of Eq. (108), yields the equations

$$-\frac{\gamma_I}{\omega_A} + \frac{\beta_h}{\epsilon} \frac{\omega}{\omega_{dm}} \ln\left(\frac{\omega_{dm}}{\omega} - 1\right) = 0 \quad (109)$$

and

$$-\frac{[\omega(\omega - \omega_{*i})]^{1/2}}{\omega_A} + \frac{\beta_h}{\epsilon} \frac{\omega}{\omega_{dm}} \pi = 0. \quad (110)$$

These can be solved for β_h ,

$$\beta_h = \frac{\epsilon \omega_{dm}}{\pi \omega_A} \left(1 - \frac{\omega_{*i}}{\omega}\right)^{1/2}, \quad (111)$$

which has real values only when $\omega > \omega_{*i}$. Substituting Eq. (111) into Eq. (109) results in a transcendental equation for ω ,

$$\gamma_I = \frac{[\omega(\omega - \omega_{*i})]^{1/2}}{\pi} \ln\left(\frac{\omega_{dm}}{\omega} - 1\right). \quad (112)$$

which is a monotonic function of ω . For $\gamma_I > 0$ we require $\omega_{*i} \leq \omega \leq \omega_{dm}/2$.

A detailed analysis [43] shows that the roots of Eq. (112) contain both fishbone and kink modes, their appearance and stability depending on the relative values of the parameters. The instability thresholds for these branches (modes) are widely separated when $\omega_{*i} \ll \omega_{dm}/2$ and $\gamma_I < \gamma_M$, where

$$\gamma_M = \frac{1}{\pi} \max\{[\omega(\omega - \omega_{*i})]^{1/2} \ln\left(\frac{\omega_{dm}}{\omega} - 1\right)\}. \quad (113)$$

This is the maximum value of γ_I , the ideal MHD growth rate, for which a solution of Eq. (112) is possible. The smaller root is near ω_{*i} , and is given by

$$\omega_1 = \frac{\omega_{*i}}{2} + \left[\left(\frac{\omega_{*i}}{2} \right)^2 + \frac{\pi^2 \gamma_I^2}{\ln^2(\omega_{dm}/\omega_1)} \right]^{1/2}. \quad (114)$$

The second root is near $\omega_{dm}/2$, and if $\gamma_I/\omega_{dm} \ll 1/\pi$, it is to a good approximation $\omega_2 = \omega_{dm}/2 \gg \omega_1$.

Therefore, under the conditions stated, for any positive value of $\gamma_I < \gamma_M$ there are two frequencies, $\omega_1 \ll \omega_2$, between which the plasma is stable. Each of these frequencies corresponds to a value of β_h ; see Eq. (111). For $\beta_h < \beta_{h1}$ the kink mode is destabilized. For $\beta_h > \beta_{h2}$, the fishbone is destabilized. This is summarized in the (γ_I, β_h) plane in Fig. 11 for the case of a slowing-down distribution with $\omega_{*i}/\omega_{dm} = 0.05$.

For the stable gap to continue to exist for resistive modes, it is necessary and sufficient to require that the arguments of the gamma functions in the dispersion relation be large (ideal limit) at the thresholds ω_1 and ω_2 [44]. This condition requires [44]

$$\gamma_I \gg \gamma_R \frac{\ln(\omega_{dm}/\gamma_I)}{\pi}, \quad (115)$$

i.e., the internal kink must be strongly ideal MHD unstable. The limits on the ideal growth rate are given by Eq. (115) and the maximum value that permits a

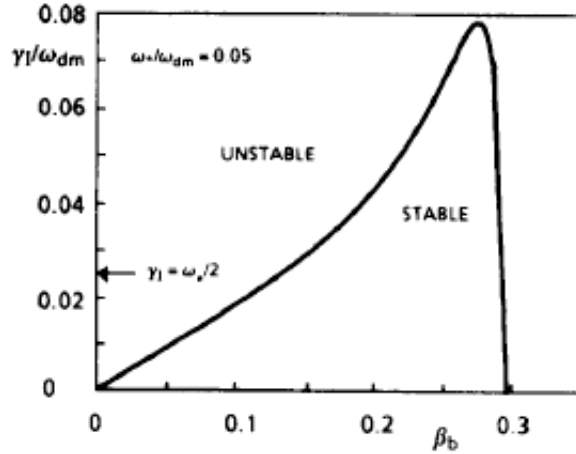


Figure 11: Stability regime in the (γ_I, β_h) plane for the case $\omega_{*i}/\omega_{dm} = 0.05$. For a given $\gamma_I > 0$, the lower limit is the kink mode and the upper limit is the fishbone [44].

solution of Eq. (112). The result is

$$\gamma_R \frac{\ln(\omega_{dm}/\gamma_I)}{\pi} \ll \gamma_I \ll \gamma_M. \quad (116)$$

The range of β_h for which both modes (resistive internal kink and fishbone) are stabilized is given approximately by [43, 44]

$$\frac{1}{\pi} \left(1 - \frac{\omega_{*i}}{\omega_1}\right)^{1/2} < \frac{\beta_h \omega_A}{\epsilon \omega_{dm}} < \frac{1}{\pi}. \quad (117)$$

The lower limit is the stabilization of the internal kink. The upper limit is the destabilization of the fishbone. For our purposes, this is the principal result. We remark that in the absence of extended MHD effects $\omega_{*i} = 0$ and the stability gap disappears. (In that case, ω_1 is the solution of the transcendental equation obtained from Eq. (114) with $\omega_{*i} = 0$.) However, it should be remembered that Eq. (117) was derived under the assumption that the threshold frequencies ω_1 and ω_2 are widely separated, so that this conclusion must be tested by a more detailed analysis.

The result also depends on S , the Lundquist number, being sufficiently large. This condition is approximately [43]

$$S \gg \frac{\ln^3(\omega_{dm}/\gamma_I) \omega_A^3}{\pi^2 \gamma_I^3}. \quad (118)$$

Note that a condition on S not being “too large” is that γ_I be large, but still small compared with $\omega_{dm}/4\pi$ [43]. A more detailed analysis reveals that $S > S_{crit}$, where critical value is [44]

$$S_{crit} = \left(\frac{\omega_A}{\gamma_M}\right)^3. \quad (119)$$

There is also a critical value of β_h , given by

$$\beta_{hc} = \frac{5\epsilon \omega_{*i} \omega_{dm}}{4\pi \hat{\omega}_{*e} \omega_A} \left(\frac{\gamma_R}{\omega_I}\right)^2. \quad (120)$$

Stabilization requires $\beta_h > \beta_{hc}$.

The stability as a function of the hot particle density is summarized in Fig 12 for two values of S [43]. These data were produced from a numerical solution of the full dispersion relation, Eq. (107), for parameters approximating a hydrogen minority species in JET, using a slowing down distribution and assuming $\gamma_I = 1.4 \times 10^4$ / sec. The horizontal axis is the hot particle density, and the vertical axis is the growth rate. For $S = 10^6$ the growth rate of kink mode is reduced but not completely stabilized; presumably the fishbone appears at higher hot particle

density. However, for $S = 10^7$ a stable gap for $1.4 \times 10^{11} < n_h < 1.95 \times 10^{11}$ appears between the kink and fishbone modes. This is the “sawtooth-free gap”.

“Perhaps it seems strange that to achieve stabilization using trapped particles the kink mode must be above its ideal threshold ($\gamma_I > 0$), but this is understandable in that it is precisely this instability that preserves the ideal character of the mode. In the resistive limit the mode cannot be stabilized and for small values of S the gap ... vanishes” [44].

The stabilization of the kink and the destabilization of the fishbone come about because of the toroidal precessional drift of the energetic trapped particles. As discussed briefly in Section 3.2.2, individual charged particle motion in a magnetic field displays several characteristic, “almost periodic” motions relative to the magnetic field, and each is associated with an “adiabatic invariant”; these are quantities that do not change, or change only slowly, in response to perturbations that are slow on the scale of the frequency of the periodic motion.

The highest frequency motion is the so-called gyro-motion about the magnetic field. Averaging over this gyro-motion yields equations that are valid on time scales long compared with the gyro-frequency and describe the motion of the “guiding center” of the particle. The adiabatic invariant associated with the motion of the guiding centers is the magnetic moment $\alpha = v_{\perp}^2/2B$, which is “almost” conserved during the period of a single gyration. As a result of this invariant, and the conservation of energy and momentum, the motion of the guiding centers can become trapped in regions of relatively weak field, as in the outboard side of a tokamak; the guiding center bounces between the so-called mirror points of the field. The remaining drifts cause the guiding center trajectory to depart from its original field line in such a way as to trace out a banana-like shape when projected in the poloidal plane. This bounce frequency is low compared with the gyro-frequency. Averaging over this bounce motion yields equations that describe the motion of the centroid of

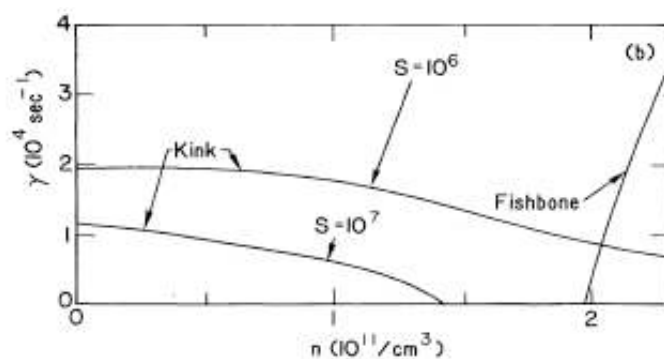


Figure 12: Growth rate vs. hot particle density for two values of the Lundquist number S using JET parameters [43].

the banana orbit. The adiabatic invariant associated with the bounce motion is called the “second adiabatic invariant”, or longitudinal invariant, $J = \oint mv_{\parallel} ds$, where the integral taken over one period of the bounce motion. The remaining periodic motion is the slow precessional drift of the banana centroids around the torus. Associated with this motion is the “third adiabatic invariant”, which is proportional to the magnetic flux linked by the orbit of the centroid as it circles the torus in the toroidal direction. This is adiabatically invariant with respect to lower frequency perturbations. The precessional frequency is the lowest of the three frequencies, and is therefore most likely to interact with MHD waves.

Now consider an MHD-like disturbance, which can have a wide range of frequencies. If the MHD frequency is near the precessional drift frequency we might expect a resonant interaction between the MHD wave and the precessing particles, which appear stationary in the frame of the wave. This is borne out by the resonant denominators appearing in Equations (89), (90), (92), (94), (99), and (101). The wave draws energy from the particles and, if there are enough particles, it appears as a growing oscillation. This is the fishbone instability. At lower frequency, such as characterized by the growth of the internal kink mode, the disturbance is too slow to interact directly with the precessing trapped particles. However, the kink attempts to rearrange the flux within the discharge, thus perturbing the third adiabatic invariant of the precessional motion. This is perturbation resisted by the energetic particles, thus lowering the growth rate of the mode. If there are sufficient energetic trapped particles, the internal kink can be completely stabilized.

If the characteristic frequencies are not sufficiently separated, or other parameters are not optimum, the number of trapped particles required to completely stabilize the internal kink (measured, for example, by β_h or n_h) is greater than the number required to destabilize the fishbone, and the discharge is always unstable to one mode or the other. However, there are parameter regimes applicable to present and future experiments where the internal kink can be completely stabilized by the hot particles before the onset of the fishbone. This accounts for the observation of extended sawtooth-free periods, terminated by “giant sawtooth” crashes.

4.2 The Porcelli Model

We now have a fairly complete picture of the linear stability of the internal kink mode in a high temperature plasma in the presence of an energetic ion population. In principle, the onset of a sawtooth crash can be predicted. In practice, the dispersion relations are complicated, and determining the stability of any particular discharge remains daunting. What is required, and would be useful, is a relatively simple way of testing a given set of equilibrium profiles (e.g., q and p) for stability with respect to the $n = 1$ mode. This could be used in conjunction with a $1 - 1/2$ -

dimensional transport model to predict the onset of a sawtooth crash, and if a sufficiently accurate model for the subsequent profile relaxation were available, a series of sawtooth crashes (or lack thereof) could be modeled.

Such a model was proposed by Porcelli, Boucher, and Rosenbluth [36], and is commonly called “the Porcelli model”. They proposed a model for both the sawtooth crash “trigger” and the profile relaxation. The trigger is based on the value of the potential energy δW , which is written as $\delta W = \delta W_{MHD} + \delta W_{KO} + \delta W_{fast}$; δW_{MHD} includes the effects of toroidicity (modified for plasma shaping, which we have not discussed), δW_{KO} is the Kruskal-Oberman correction for the effects of trapped thermal particles, and δW_{fast} represents the contribution of collisionless fast ions. These have been discussed in detail in the previous sections. The latter two contributions are stabilizing (i.e., positive), at least for standard tokamak profiles [36]. As we have seen, theoretically the relevant contributions come from inside the $q = 1$ surface, which is called the “core”; its potential energy is defined as $\delta W_{core} = \delta W_{MHD} + \delta W_{KO}$. The normalized potential energy is defined as $\delta \hat{W} \equiv -4\delta W / (s_1 \xi^2 \epsilon_1^2 R B^2)$, where $s_1 = r_1 q'(r_1)$ is the shear parameter, and $\epsilon_1 = r_1/R$ is the inverse aspect ratio, at the $q = 1$ surface. The discharge is assumed to be in the ion-kinetic regime (see Section 3.1.5), and the Porcelli model takes the internal kink growth rate (in the absence of diamagnetic or trapped particle effects) to be

$$\gamma_\rho = C_\rho(\tau) \hat{\rho}^{4/7} S^{-1/7} s_1^{6/7} \tau_A^{-1} , \quad (121)$$

where C_ρ depends on the temperature ratio $\tau = T_e/T_i$, and $\hat{\rho} = \rho_i/r_1$ is the normalized ion gyroradius. (Porcelli, et.al. [36] cite Ref. [19] for this expression. Unfortunately, I cannot find anything in Ref. [19] that vaguely resembles Eq. (121). My assumption is that it derives from Eq. (76) of Section 3.1.5, but I cannot be sure. In any case, this is what is used in the model. Further note the typo in Eq. (6) of Ref. [36], where the exponent of $\hat{\rho}$ is given as 47. I have assumed that the correct value is 4/7 but, again, I can’t be sure.) Note the very weak S dependence in this regime.

Analytic formulas that can be applied to “arbitrary” equilibrium profiles are used, although their origin is a bit fuzzy, at least to me. The normalized potential energy is

$$\delta \hat{W} = \delta \hat{W}_{Bussac} + \delta \hat{W}_{el} + \delta \hat{W}_{KO} + \delta \hat{W}_{fast} , \quad (122)$$

where the ideal MHD potential energy is $\delta \hat{W}_{MHD} = \delta \hat{W}_{Bussac} + \delta \hat{W}_{el}$; the toroidal expression is approximately [see, for example, Eqs. (78) and (79)]

$$\delta \hat{W}_{Bussac} = -c_{MHD} \epsilon_1^2 \left(\beta_{p1}^2 - \beta_{pc}^2 \right) , \quad (123)$$

with

$$c_{MHD} = \frac{9\pi}{s_1} \left(l_{i1} - \frac{1}{2} \right) , \quad (124)$$

l_{i1} is the plasma internal inductance at the $q = 1$ surface (see [10, p. 122] for the cylindrical version), β_{p1} is the poloidal beta of the core + energetic particle pressure within the $q = 1$ surface, and

$$\beta_{pc} = 0.3 \left(1 - \frac{5r_1}{3a} \right) , \quad (125)$$

where a is the “average” minor radius; the “elongation” term is

$$\delta\hat{W}_{el} = -c_{el} \left(\frac{\kappa_1 - 1}{2} \right)^2 , \quad (126)$$

where κ_1 is the geometric elongation of the $q = 1$ surface and

$$c_{el} = \frac{18\pi}{s_1} \left(l_{i1} - \frac{1}{2} \right)^2 ; \quad (127)$$

the Kruskal-Oberman term (see Eq. (82), Section 3.2.3, and the following discussion) is

$$\delta\hat{W}_{KO} = 0.6 \frac{c_p \epsilon_1^{1/2} \beta_{i0}}{s_1} ; \quad (128)$$

and the fast (or energetic) particle term is

$$\delta\hat{W}_{fast} = c_f \frac{\epsilon_1^{1/2} \beta_{pf}^*}{s_1} , \quad (129)$$

where

$$\beta_{pf}^* = -\frac{8\pi}{B_p^2(r_1)} \int_0^1 dx x^{3/2} \frac{dp_f}{dx} , \quad (130)$$

with $x = r/r_1$ is a measure of the fast particle pressure gradient within the $q = 1$ surface. (According to Ref. [46], these expressions for $\delta\hat{W}_{fast}$ are obtained “... using a simplified isotropic distribution function with zero orbit widths, appropriate for ITER α -heated discharge scenarios”.)

For a given equilibrium profile, a sawtooth crash is triggered (i.e., the profile becomes unstable to the internal kink mode) whenever any one of the following conditions is met:

$$-\delta\hat{W}_{core} > c_h \omega_{dm} \tau_A , \quad (131)$$

$$-\delta\hat{W} > 0.5\omega_{*i}\tau_A , \quad (132)$$

or

$$-c_\rho\hat{\rho} < -\delta\hat{W} < 0.5\omega_{*i}\tau_A \text{ and } \omega_{*i} < c_*\gamma_\rho , \quad (133)$$

along with the auxiliary condition $\omega_{dm} > \omega_{*i}$. Here, the expressions for the various contributions to $\delta\hat{W}$ are given by Eqs. (123) - (130), γ_ρ by Eq. (121), ω_{dm} is the precessional drift frequency of the energetic ions, and c_h , c_ρ , and c_* are “constants of order unity”.

Equation (131) is the condition for loss of energetic particle stabilization; $\delta\hat{W}_{core}$ includes the effects of the fluid and thermal trapped particles, but not fast particles. “The stabilizing influence of high energy ions is a consequence of the third adiabatic invariant, i.e., the magnetic flux linked through the fast trapped ion precessional drift orbits. This non-MHD constraint becomes relevant when the high energy trapped particles complete many orbits within a characteristic perturbation time of order $|\delta\hat{W}_{core}^{-1}|\tau_A$.” [36]. Equation (131) follows.

Equation (132) is equivalent to $\omega_* > 2\gamma$, which is the well known condition for stability in the presence of two-fluid (ion diamagnetic) effects (see Section 3.1.4). (In this case, γ refers to the growth rate of the mode including all contributions to $\delta\hat{W}$, not just MHD.) According to Ref. [46], it “represents the destabilization of the ideal mode modified by including trapped fast ion stabilization but where finite ion diamagnetic frequency effects are insufficient to stabilize the mode.”

I do not understand the origin of Eq. (133). Again, according to Ref. [46], it “represents the destabilization of the nonideal resistive or ion-kinetic mode”. The best I can do is to quote from what I think is the relevant passage of Ref. [36]: “In the asymptotic limit $-\delta\hat{W} > \max[\hat{\rho}, \omega_{di}\tau_A/2] \equiv -\delta\hat{W}_{crit}$ ($\hat{\rho} = \rho_i/r_1$ is the nondimensional ion Larmor radius) “where layer physics effects become unimportant, the internal kink growth rate normalized to the Alfvén time reduces to $\gamma\tau_A \approx -\delta\hat{W}$.”

“Layer physics plays an important role when $|\delta\hat{W}| \leq |\delta\hat{W}_{crit}|$. In particular, when $|\delta\hat{W}| < \hat{\rho}$, the $m = 1$ mode structure changes its nature from that of a global internal kink to that of a drift-tearing mode localized near the $q = 1$ surface, which is normally stable because of kinetic layer effects at high plasma temperatures. In this context, the electron drift frequency near the $q = 1$ surface, ω_{*e} , also plays a role, and we shall assume that $\omega_{*e} \sim -\omega_{*i}$. In the interval $-\hat{\rho} < -\delta\hat{W} < -\delta\hat{W}_{crit}$, the $m = 1$ mode can be stabilized by ion diamagnetic and electron drift wave frequency effects, allied with effective plasma viscosity (a sink of momentum). The stabilization criterion requires values of ω_{*i} a few times larger than the growth rate evaluated at $\omega_{*i} = 0$.”

I couldn't have said it better myself!

Using Eq. (121), the inequality $\omega_{*i} < c_* \gamma_\rho$ in Eq. (133) can be transformed into a critical shear condition for instability, $s_1 > s_{crit}$, where s_{crit} is given by Eq. (15a) in Ref. [36]; it is of no detailed interest to us. However, it is important to note that the shear at the $q = 1$ surface, s_1 , appears in the denominator of both $\delta\hat{W}_{fast}$ and $\delta\hat{W}_{KO}$, which are the stabilizing terms. We thus expect that the stabilization of the internal kink will be strongly influenced by this parameter; increases are destabilizing. This will be borne out in Section 4.3.

The Porcelli model is based on simple analytic approximations to detailed linear stability results. In principle, the relevant terms in $\delta\hat{W}$ could be computed with a linear MHD stability code. It is interesting that this approach is rejected in Ref. [36]: “However, even though feasible, it is impractical to interface such a code with a transport code”, the primary reason being the uncertainties in the integrity of the profiles produced by the transport code itself (see [36, pp. 2168ff]). Since this is precisely one of the goals of the proposed Fusion Simulation Project, one hopes the state of computing has advanced significantly since 1996!

Of course, once instability is triggered, neither linear theory nor transport modeling can tell us anything about the final state. As mentioned previously, Kadomtsev [6] proposed a model for the final state based on complete reconnection. Reference [36] states that “Kadomtsev’s model is not always consistent with experimental data, even though observations from different tokamak experiments are somewhat conflicting”, and they propose a model based on “incomplete relaxation”. Fortunately, we are approaching a time when we can not only couple linear stability and transport codes, but also nonlinear MHD and gyrokinetic models with the potential to produce a self-consistent picture of sawtooth stabilization, destabilization, and nonlinear relaxation.

4.3 Validation of the Sawtooth Model

The Porcelli models makes predictions of the onset of a sawtooth crash for a given plasma configuration. As we have seen, these predictions are based on approximate analytic estimates of various terms in the plasma potential energy $\delta\hat{W}$. If it is accurate, it would be extremely useful for both design scenarios and performance evaluation in ITER.

In order to assess the efficacy of this model, its predictions need to be compared directly with better estimates of the various terms in $\delta\hat{W}$ for a real experimental discharge for which accurate and high frequency equilibrium reconstructions are available. Such a discharge is DIII-D shot 96043 [45]. This is a tokamak discharge with neutral beam injection and fast wave (RF) heating. It exhibits both “normal” and “giant” sawtooth oscillations. The time history of several experimental parameters is shown in Fig. 13. A 2.7 MW neutral beam that produces 80 KeV ions is initiated at $t \approx 1.25$ seconds; 1250 milliseconds. This produces an energetic

ion population having a slowing-down distribution with $E_m = 80$ KeV. The resulting heating induces a series of relatively small sawtooth oscillations, which can be seen in the electron temperature in the range $1.5 < t < 1.8$ seconds. These are the “normal” sawteeth. At $t = 1.8$ seconds, 60 MHz fast wave (RF) heating was applied. This accelerated some of the energetic ions to energies of several hundred KeV, much higher than the injection energy. As seen in the electron temperature, the interval between the sawtooth crashes lengthened, and their amplitude increased; there are noticeable drops in the stored energy at each crash. These are the “giant” sawteeth. Presumably, the increase in $\delta\hat{W}_{fast}$ due to the more energetic RF-accelerated beam particles stabilizes the internal kink mode in the intervals between sawtooth crashes.

Reference [46] reports a detailed study of one of the extended stable periods between giant sawtooth crashes. The particular interval chosen was $1800 < t < 2040$ msec., as shown on Fig. 14. Equilibrium reconstructions providing details of the evolving plasma and magnetic field profiles are available throughout this period. These can be used to compute the contributions to $\delta\hat{W}$ by several different methods, and compare the predictions of the Porcelli model with the actual onset of the sawtooth crash in the experiment.

For example, values of $\delta\hat{W}_{mhd}$, the MHD or fluid contribution, at various times

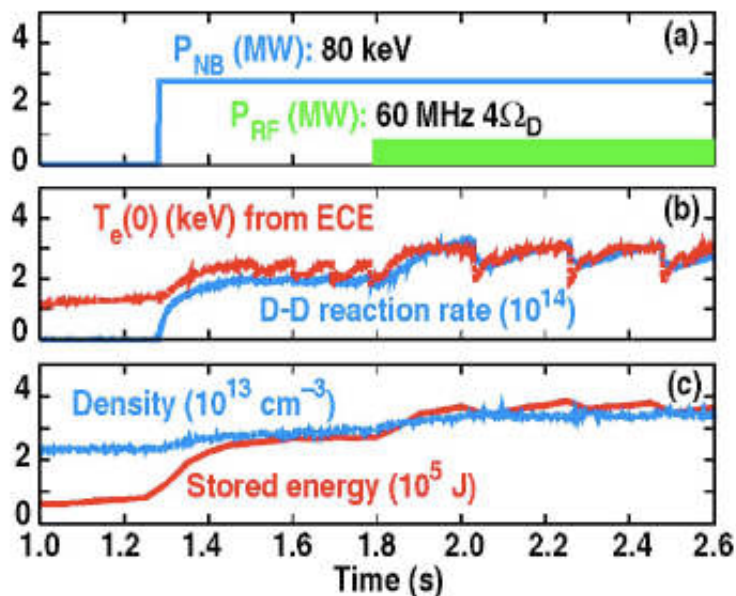


Figure 13: Time history of experimental parameters for DIII-D discharge 96043. Top: Input power. Center: Electron temperature and D-D reaction rate. Bottom: Density and stored energy. [46].

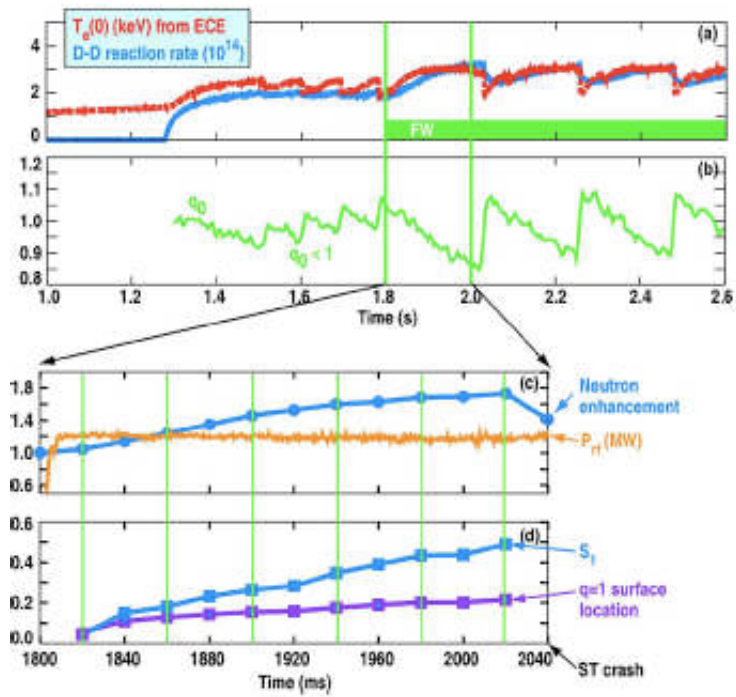


Figure 14: Blow up of the specific sawtooth interval ($1800 < t < 2040$ msec.) chosen for detailed study. Equilibrium reconstructions are available throughout this period (at the vertical lines in the lower two plots) [46].

in the quiescent interval are shown in Fig. 15. The curve labeled $\delta\hat{W}_{Bussac}$ is from Eq. (123), which is part of the original Porcelli model. The curve labeled $\delta\hat{W}_{Martynav}$ ([sic]; it should be “Martynov”) is from a different, and supposedly more accurate, analytic model [47]. The curve labeled $\delta\hat{W}_{GATO}$ are results from the linear stability code GATO [48] applied to the reconstructed equilibrium profiles at each time. While all three models predict an MHD unstable plasma, $\delta\hat{W}_{MHD} < 0$, the computational (and presumably more accurate and realistic) result from GATO indicates significantly more instability drive than either of the analytic models.

Presumably, the stabilization of the unstable MHD mode comes from the contributions $\delta\hat{W}_{KO}$ and $\delta\hat{W}_{fast}$. For all cases, $\delta\hat{W}_{KO}$, the contribution of the thermal trapped particles, is computed using Eq. (128), as in the Porcelli model. It is found to be small and positive. The contribution from the fast trapped particles, $\delta\hat{W}_{fast}$, is computed from Eqs. (129) and (130). The fast particle pressure is determined by accelerating test particles with the ORBIT-RF code [49] using the fast wave fields computed by the TORIC code [50]. The resulting distribution function for the fast particles consist of a slowing down distribution for $E < E_m = 80$ KeV, and a high energy tail extending to several hundred KeV. It is this high energy tail that provide for the stabilization of the mode. (Reference [9] states unequivocally: “Apparently, tail formation is a necessary, but not sufficient, condition for

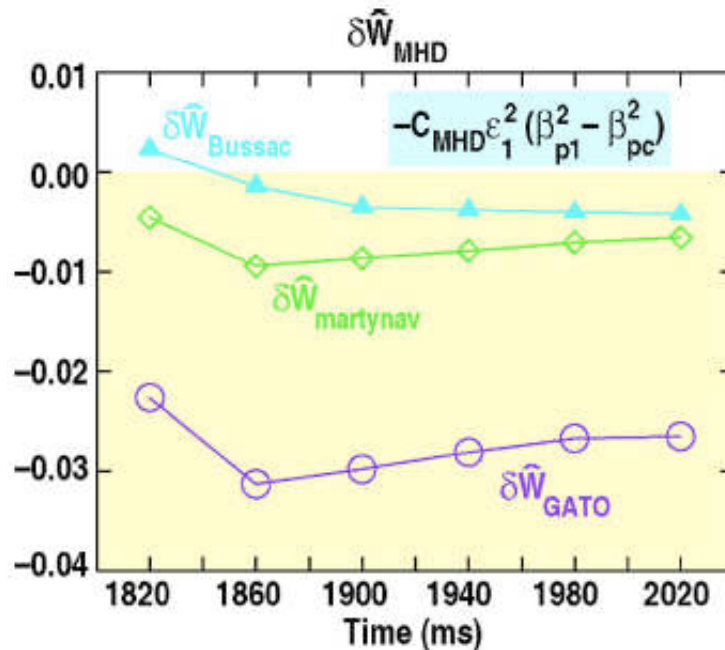


Figure 15: MHD contribution to the potential energy using three different models during a period between giant sawtooth crashes) [46].

enhanced sawtooth stability.” However, we have seen in Section 4.1 that, at least in theory, stabilization can be achieved with a slowing down distribution.)

In Fig. 16 are plotted the time history of the various contributions to $\delta\hat{W}$ during the period leading up to the sawtooth crash. In the upper figure, $\delta\hat{W}_{MHD} = \delta\hat{W}_{GATO}$, and in the bottom figure $\delta\hat{W}_{MHD} = \delta\hat{W}_{Martynov}$. In the top figure, $\delta\hat{W}$

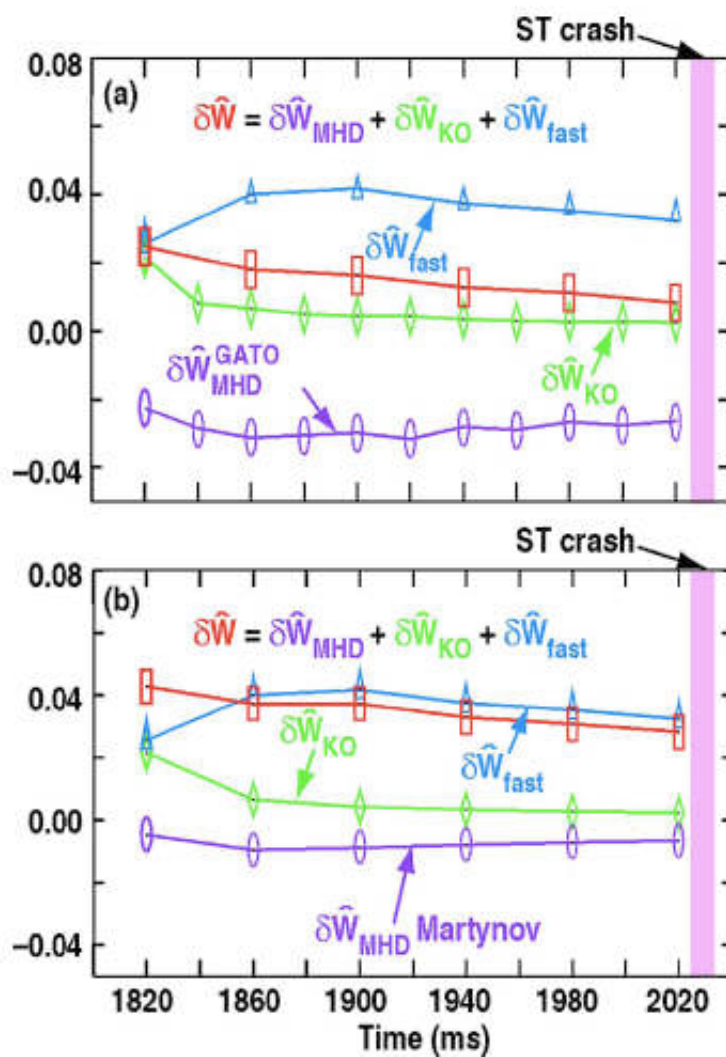


Figure 16: Evolution of the total potential energy leading up to the sawtooth crash, Top: $\delta\hat{W}_{MHD} = \delta\hat{W}_{GATO}$. Note that $\delta\hat{W}$ approaches 0 at the sawtooth crash. This is due to large MHD drive and a decrease in fast particle stabilization. Bottom: $\delta\hat{W}_{MHD} = \delta\hat{W}_{Martynov}$. Here $\delta\hat{W}$ remains positive throughout because of insufficient MHD drive. [46].

approaches 0 at the sawtooth crash due to the large MHD drive and a decrease in fast particle stabilization. In the bottom figure $\delta\hat{W}$ remains positive throughout because of insufficient MHD drive. This indicates that an accurate estimate of the MHD (or fluid) drive for the instability is essential for the prediction of the sawtooth onset.

The destabilization of the internal kink and the onset of the sawtooth crash is due to a decrease in $\delta\hat{W}_{fast}$. The time histories of $\delta\hat{W}_{fast}$, β_{ph} , the poloidal beta of the hot particles as determined by the ORBIT-RF code, and the shear parameter $s_1 = r_1 q'(r_1)$, are plotted in Fig. 17. The critical value of shear is also plotted (see Section 4.2). The particle β saturates as the distribution function reaches steady state, after which $\delta\hat{W}_{fast}$ displays a steady decrease. This is primarily due to the steady increase in the shear at the $q = 1$ surface, which appears in the denominator of $\delta\hat{W}_{fast}$ (see Eq. (129)). It is this increase in shear, as opposed to an increase in β_{ph} , that is responsible for the loss of energetic particle stabilization and the triggering of the sawtooth crash.

Finally, the specific criteria in the Porcelli model for triggering a sawtooth crash can be evaluated. This is shown in Fig. 18 using $\delta\hat{W}_{MHD} = \delta\hat{W}_{GATO}$. The

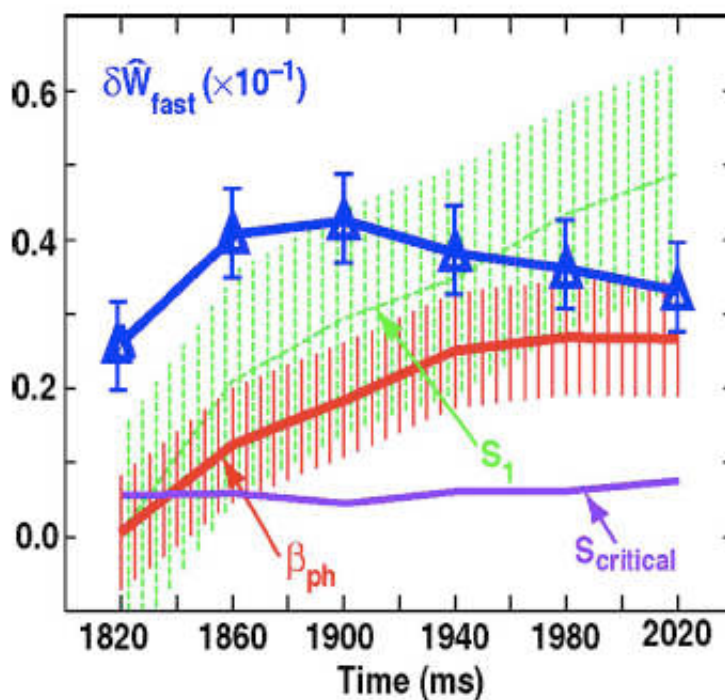


Figure 17: Fast particle potential energy, fast particle β , and the shear parameter during the period before the sawtooth crash [46].

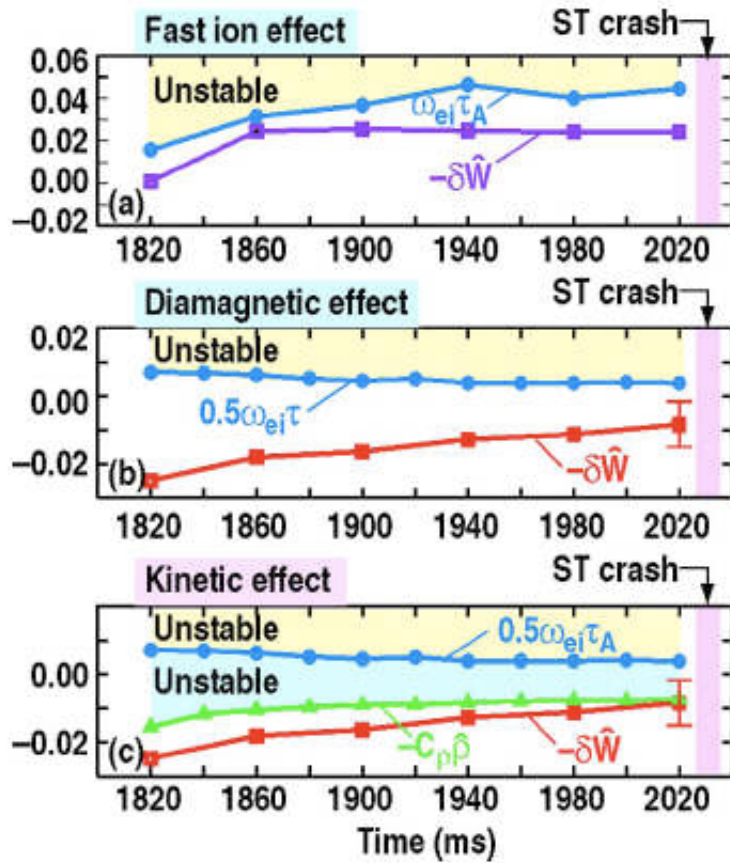


Figure 18: Evaluation of the three sawtooth triggers in the Porcelli model. Top: The fast ion effect, Eq. (131). Middle: The diamagnetic effect, Eq. (132). Bottom: The kinetic effect, Eq. (133). Note that some of the curves are mislabeled [46].

fast ion effect, Eq. (131), can be the trigger if the purple curve lies above the blue curve. (Note that the blue curve should be labeled $\omega_{dm}\tau_A$.) The diamagnetic effect, Eq. (132), can be the trigger if the red curve lies about the blue curve (which should be labeled $0.5\omega_{*i}\tau_A$). The kinetic effect, Eq. (133), can be the trigger if the red curve lies between the green and blue curves (which should be labeled $\omega_{*i}\tau_A$). Clearly, the onset of the crash corresponds to the trigger $-\delta\hat{W} > -c_\rho\hat{\rho}$, the first of Eq. (133). “This result implies that fast wave accelerated trapped beam ions are crucial to stabilizing the sawtooth instability and extending the period. Nevertheless, eventually, at the end of this cycle, the sawtooth crash is triggered by the resistive internal kink mode in the ion-kinetic regime.” [46]

Therefore, the Porcelli model provides a guide as long as the individual terms are computed with sufficient accuracy. This likely implies that the application of integrated plasma simulation models will be essential to gaining an understanding of the sawtooth behavior of modern tokamaks. Of course, this only addresses the trigger mechanism, which relies on *linear* theory. The state of the relaxed equilibrium after the crash, and the fate of the energetic particles (be they beam ions or α -particles) require coupling of *nonlinear* computational models of extended MHD and particle dynamics. This is The Future.

4.4 Future Directions

While the results of Ref. [46] suggest that something like the Porcelli model [36] may provide a guide to the onset of the sawtooth crash in modern tokamaks, they also clearly show that using it blindly within the context of a transport model can lead to faulty predictions. First, the MHD (or fluid) contribution to the potential energy must be computed accurately, accounting for the local details of the profiles, the non-circular poloidal geometry and the boundary conditions. Second, the details of the energetic trapped particle distribution function must be known accurately. These are not possible within the context of analytic or semi-analytic models for $\delta\hat{W}_{MHD}$ and $\delta\hat{W}_{fast}$. At a minimum, the low order dimensional transport model must be directly and intimately coupled with a linear MHD stability code, such as GATO, and perhaps even an RF/kinetic computational model such as TORIC/ORBIT-RF. This is a challenging prospect, and, even if successfully implemented, it would remain silent on the nonlinear aspects of the crash, such as the state of the relaxed profiles, the loss of stored energy and its deposition on the walls, and the fate of the energetic particles. Addressing these important issues will eventually dictate abandoning the transport approach and employing a three-dimensional nonlinear extended MHD code, such as NIMROD [51, 52] as the core computational component.

The NIMROD code solves the three-dimensional nonlinear extended MHD equations [52]. The geometry must have one periodic dimension (such as the

toroidal direction in a tokamak), but is otherwise arbitrary. The plasma can extend to the wall, or be surrounded by a vacuum with an enclosing conducting boundary. (Resistive wall boundary conditions are being implemented.) It can be run in a linear mode, so linear MHD and extended MHD stability can be assessed efficiently. An important issue for the extended MHD model is that of closures [52], i.e., expressions for the higher order velocity moments of the distribution function in terms of the lower order moments. NIMROD incorporates the full Braginskii (collisional) closure model [53] as a default, and models for neo-classical closures (valid for low collisionality) are being developed [54], and NIMROD is being coupled to RF power deposition models to simulate the stabilization of resistive and neo-classical tearing modes with ECCD [55].

Of importance to the study of giant sawteeth, NIMROD contains a gyrokinetic model for a minority, non-Maxwellian (energetic) ion species [52, 56]. The evolution of the perturbed distribution function is computed by integrating the gyrokinetic equations in the evolving magnetic field of the background plasma, and its effect on the evolution of the fluid is captured by computing their contribution to the ion stress tensor (see Eq. (86), Section 3.2.4) by direct velocity space integration. This model has been benchmarked against previous known results [57], and has already demonstrated complete stabilization of the internal kink mode [56].

A systematic study of the effect of an energetic trapped particle population on the stability and evolution of the internal kink mode and resulting sawtooth crash has begun. Because of the availability of both experimental and theoretical (computational) results, the sequence of equilibrium reconstructions from DIII-D discharge 96043 [45, 46] is being used. The results of this study will provide excellent verification and validation tests for the integrated simulation model of NIMROD, and (hopefully) will lead to advances in large scale computations and understanding of the physics of giant sawteeth.

We begin by studying the linear stability of discharge 96043 at $t = 1900$ msec., where the stabilizing effect of the energetic trapped particles is maximum (see Fig. 17). For these calculations, NIMROD was run as a linear stability code, and only the MHD model was used. One issue with these calculations is the choice of “equilibrium” distribution function for the energetic ions. The present NIMROD particle model uses a slowing down distribution with maximum energy E_m . In discharge 96043, the energetic ions are injected with a neutral beam with $E_m = 80$ KeV, and are then accelerated to much higher energy by RF radiation. As discussed in Section 4.3, this leads to a distribution function that is a superposition of a slowing down distribution with $E_m = 80$ KeV, and a high energy tail extended to several hundred KeV. The principal stabilization of the kink comes from this high energy tail [46]. NIMROD does not yet incorporate such a model for the equilibrium distribution. We have therefore begun by performing generic studies

using the slowing down distribution, and examining the stabilization properties for different values of both the injection energy E_m and the hot particle beta β_{hp} . (A primary assumption is that the presence of the energetic particles does not affect the MHD equilibrium force balance $\nabla p = \mathbf{J} \times \mathbf{B}$ as given by the equilibrium reconstruction.)

The *preliminary* results are shown in Fig. 19, where we plot the growth rate of the internal kink mode in DIII-D shot 96043 as a function of β_{hp}/β for two slowing down distributions, one with $E_m = 41.75$ KeV and the other with $E_m = 281$ KeV. Both the plasma and the beam are deuterium. The Lundquist number is $S = 1.7 \times 10^7$, and the resistive MHD growth rate (with $\beta_{hp} = 0$) is $\gamma_R = 3.29 \times 10^4$ /sec.. At 41 KeV, the precession frequency is $\omega_{pd} = 5 \times 10^4$

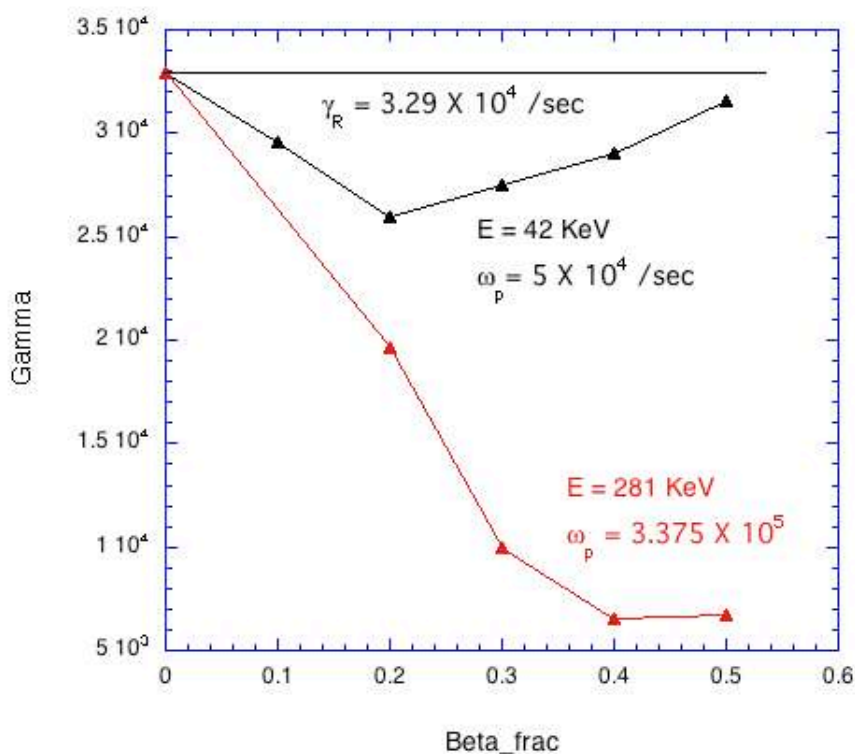


Figure 19: Growth rate of the internal kink mode in DIII-D shot 96043 as a function of β_{hp}/β for two slowing down distributions with $E_m = 41.75$ KeV and $E_m = 281$ KeV.

/sec., so that $\gamma_R/\omega_{pd} = 0.66$; at the $q = 1$ surface, $\omega_{pd} = E_m/m_h\omega_{hc}Rr_1$, so that the precession frequency is proportional to the energy. The growth rate and the precession frequency are not widely separated, and little stabilization is expected. (Recall that it is the conservation of the third adiabatic invariant that is responsible for the stabilization.) However, for 281 KeV, $\gamma_R/\omega_{pd} = 0.097$, so they are separated by a factor of 10. Nonetheless, there is no stable gap for either value of E_m . These results are converged in both spatial and temporal resolution, as well as in the number of particles. (At high energy convergence required 10^7 particles.) There is a minimum in the growth rate at $\beta_f \equiv \beta_{hp}/\beta \approx 0.2$. Presumably, for $E_m = 41$ KeV, $\beta_f < 0.2$ represents partial stabilization of the internal kink by energetic particles, and $\beta_f > 0.2$ represents destabilization of the fishbone mode. Perhaps even larger separation between γ_R and ω_{pd} is required to achieve stabilization. Or perhaps, as speculated in Ref. [9], a true energetic tail is required of the hot particle distribution function.

In Fig. 20 we plot the growth rate as a function of the injection energy for $\beta_f = 0.2$, the minimum in Fig. 19. (The case with $E_m = 140$ KeV required 10^7 particles for convergence.) Even with $E_m = 140$ KeV, the growth rate and the precession frequency are not widely separated. However, the growth rate does not decrease linearly with energy, as reported in Ref. [56], and there are indications that stabilization may not occur at even higher values of E_m . Perhaps this is because, even if the third adiabatic invariant is well conserved for individual particles, there are insufficient energetic particles to resist the flux change induced by the current perturbation caused by the internal kink. Runs at high energy with increased β_f are underway.

The preliminary calculations reported here are challenging, and they raise several questions.

What is the required separation between the resistive growth rate and the precession frequency (energy) of the hot particles to achieve stability? So far we have only gone to a few hundred KeV for the injection energy of the hot particles, and this gives $\omega_{pd}/\gamma_R \simeq 10$. Theory requires $\omega_{pd}/\gamma_R \gg 1$. Calculations with $E_m > 100$ KeV have required in excess of 10^7 particles. Can we afford to go higher? And, does the β_f required for stability increase with E_m ?

What is the role of the hot particle distribution function? The present algorithm assumes a slowing down equilibrium distribution function for the hot particles. How important is the form of the distribution function, as opposed to its maximum energy, to stabilization?

What is the role of extended MHD effects on linear stability? Analytically, the stabilization criterion for the internal kink includes diamagnetic effects (see Eq. (117)). The present calculations only include the resistive MHD Ohm's law. Will it be necessary to extend the particle model to use the extended MHD Ohm's

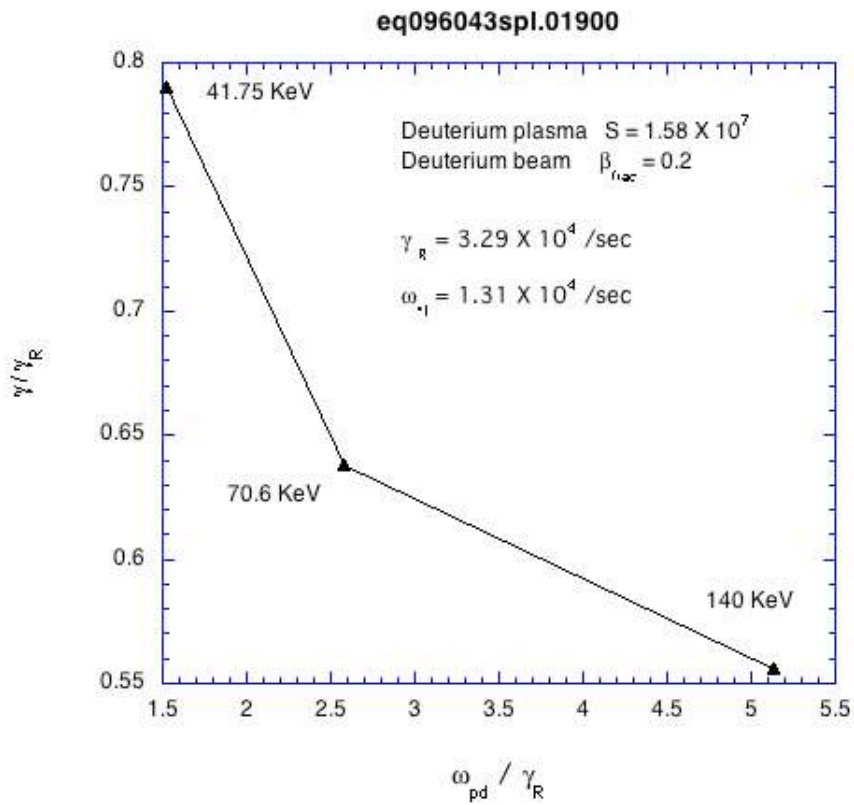


Figure 20: Growth rate of the internal kink mode in DIII-D shot 96043 as a function of E_m (or equivalently ω_{pd}) for $\beta_f = 0.2$.

law? Further, it is well known that, in the absence of extended MHD (diamagnetic) effects, tokamak plasmas are predicted to be increasingly unstable at high n (toroidal mode number); extended MHD is required to stabilize these modes and allow nonlinear computations to proceed. I suspect that, for one reason or another, extended MHD will have to be addressed by the kinetic model in NIMROD.

How do we include the effects of thermal trapped particles? The stabilizing effect thermal trapped particles are encapsulated in δW_{KO} , the Kruskal-Oberman term. However, these particles are part of the *majority* ion species that is modeled by the fluid equations. How is their presence to be captured? Are they described by so-called neo-classical effects? Reference [46] found their effect to be small, but they could be important in other configurations.

Is there a critical value of the Lundquist number? Theoretically, the Lundquist number must exceed a critical value for stabilization (see Eq. (119)). The present results have been obtained with $S = 1.7 \times 10^7$, which is quite large for computation but quite small for a modern tokamak. Is it large enough, or is the lack of stabilization seen so far simply a result of having S too low?

Can we afford to compute in the required parameter regime? Large hot particle energy, which is required for separation between the growth rate and the precession frequency, require many particles for convergence of the gyrokinetic model. So far, linear calculations with 10^7 particles have been able to proceed practically because of parallelization of the particle algorithm in the poloidal plane. Is this sufficient for even higher energies, or more toroidal modes (as required for nonlinear calculations). How much code development will be required for the particle algorithm to be practical for these problems?

Can nonlinear calculations be done? We have very little experience here, especially with large scale modes in toroidal geometry. The present calculations will push the envelope for nonlinear computation, and hopefully will promote further advances in both numerical and computational algorithms.

But first, I'd just like to see complete linear stabilization of the internal kink in DIII-D shot 96043!

References

- [1] S. C. Jardin, presentation at CEMM planning meeting, General Atomics, August 21, 2002. (This presentation does not seem to be on the CEMM web site. I can make it available on request.)
- [2] S. von Goeler, W. Stodiek and N. Sautoff, Phys. Rev. Letters **33**, 1201 (1974).
- [3] V. D. Shafranov, Sov. Phys. Tech. Phys. **15**, 175 (1970).

- [4] Zhixuan Wang, private communication (2012).
- [5] M. N. Rosenbluth, R. Y. Dagazian, and P. H. Rutherford, *Phys. Fluids* **16**, 1894 (1973).
- [6] B. B. Kadomtsev, *Sov. J. Plasma Phys.* **1**, 389 (1975).
- [7] M. N. Bussac, D. Edery, R. Pellat and J. L. Soule, in *Plasma Physics and Controlled Nuclear Fusion Research 1976*, p. 617, IAEA-CN-35/B3, IAEA, Vienna, 1977.
- [8] D. J. Campbell, et al., *Phys. Rev. Letters* **60**, 2148 (1988).
- [9] W. W. Heidbrink, E. D. Fredrickson, T. K. Mau, C. C. Petty, R. I. Pinsky, M. Porkolab and B. W. Rice, *Nucl. Fusion* **39**, 1369 (1999).
- [10] J. P. Freidberg, *Ideal Magnetohydrodynamics*, Plenum Press, New York, 1987.
- [11] B. Coppi, R. Galvão, R. Pellat, M. N. Rosenbluth, and P. Rutherford, *Sov. J. Plasma Phys.* **2**, 533 (1976).
- [12] G. Ara, B. Basu, B. Coppi, G. Laval, M. N. Rosenbluth, and B. V. Waddell, *Ann. Physics* **112**, 443 (1978).
- [13] Carl M. Bender and Steven A. Orszag, *Advanced Mathematical Methods for Scientists and Engineers*, Springer Science, New York, 1999.
- [14] H. P. Furth, J. Killeen, and M. N. Rosenbluth, *Phys. Fluids* **6**, 459 (1963).
- [15] M. Abramowitz and I. Stegun, *Handbook of Mathematical Functions*, Dover, New York, 1972.
- [16] G. Arfken, *Mathematical Methods for Physicists*, Second Ed., Academic Press, New York, 1970.
- [17] E. T. Whittaker and G. N. Watson, *A Course of Modern Analysis*, Cambridge University Press, Cambridge, 1969.
- [18] F. Pegoraro and T. J. Schep, *Plasma Phys. Cont. Fusion* **28**, 647 (1986).
- [19] F. Pegoraro, F. Porcelli, and T. J. Schep, *Phys. Fluids B* **1**, 364 (1989).
- [20] R. P. Feynman, R. B. Leighton, and M. Sands, *The Feynman Lectures on Physics*, Addison-Wesley, Reading, 1963.
- [21] B. V. Waddell, M. N. Rosenbluth, D. A. Montecello, and R. B. White, *Nucl. Fusion* **16**, 528 (1976).

- [22] A. Sykes and J. A. Wesson, Phys. Rev. Letters **37**, 140 (1976).
- [23] R. D. Hazeltine, G. T. Hsu, and P. J. Morrison, Phys. Fluids **30**, 3204 (1987).
- [24] A. Y. Aydemir, Phys. Fluids B **4**, 3469 (1992).
- [25] M. N. Bussac, R. Pellat, D. Edery, and J. L. Soule, Phys. Rev. Letters **35**, 1638 (1975).
- [26] A. Sykes and J. A. Wesson, Nucl. Fusion **14**, 645 (1974).
- [27] W. Kerner, Princeton University, PPL Report MATT-1229 (1976).
- [28] D. Berger, R. Gruber, and F. Troyon, *Controlled Fusion and Plasma Physics*, Proceedings of the Eighth European Conference, Prague, Vol. I, p. 51 (1977).
- [29] J. A. Wesson, 12th European Conference on Controlled Fusion and Plasma Physics, Budapest (1985).
- [30] P. Helander and D. J. Sigmar, *Collisional Transport in Magnetized Plasmas*, University Press, Cambridge, 2002.
- [31] H. Goldstein, *Classical Mechanics*, Addison-Wesley, Reading, 1950.
- [32] R. D. Hazeltine and J. D. Meiss, *Plasma Confinement*, Addison-Wesley, Redwood City, 1992.
- [33] I. Berenstein, E. Frieman, M. Kruskal, and R. Kulsrud, Proc. Roy. Soc (London) **A244**, 17 (1958).
- [34] M. D. Kruskal and C. R. Oberman, Phys. Fluids **1**, 275 (1958).
- [35] T. M. Antonsen, Jr., and Anders Bondeson, Phys. Fluids B **5**, 4090 (1993).
- [36] F. Porcelli, D. Boucher, and M. N. Rosenbluth, Plasma Phys. Cont. Fusion **38**, 2163 (1996).
- [37] M. N. Rosebluth, S. T. Tsai, J. W. VanDam, and M. G. Engquist, Phys. Rev. Letters **51**, 1967 (1983).
- [38] K. McGuire, et al., Phys. Rev. Letters **50**, 891 (1983).
- [39] Liu Chen, R. B. White, and M. N. Rosenbluth, Phys. Rev. Letters **52**, 1122 (1984).
- [40] H. Biglari and Liu Chen, Phys. Fluids **29**, 1760 (1986).

- [41] J. Jacquinet, et al., in *Proceedings of the Eleventh International Conference on Plasma Physics and Controlled Nuclear Fusion Research, Kyoto, Japan, 1986* Vol. 1, p449, IAEA, Vienna, 1987.
- [42] R. B. White, P. H. Rutherford, P. Colestock and M. N. Bussac, *Phys. Rev. Letters* **60**, 2038 (1988).
- [43] R. B. White, M. N. Bussac, and F. Romanelli, *Phys. Rev. Letters* **62**, 539 (1989).
- [44] R. B. White, F. Romanelli, and M. Bussac, *Phys. Fluids B* **2**, 745 (1990).
- [45] J. L. Luxon, *Nucl. Fusion* **42**, 614 (2002).
- [46] M. Choi, A. D. Turnbull, V. S. Chan, et al., *Phys. Plasmas* **14**, 112517 (2007).
- [47] A. Martynov, J. P. Graves and O. Sauter, *Plasma. Phys. Cont. Fusion* **47**, 1743 (2005).
- [48] L. C. Bernard, F. J. Helton and R. W. Moore, *Comput. Phys. Commun.* **21**, 377 (1981).
- [49] M. Choi, V. S. Chan, R. I. Pinsky, et al., *Nucl. Fusion* **46**, S409 (2006).
- [50] M. Brambilla, *Plasma Phys. Cont. Fusion* **41**,1 (1999).
- [51] C. R. Sovenic, A. H. Glasser, T. A. Gianakon, et al., *J. Comput. Phys.* **195**, 355 (2004).
- [52] D. D. Schnack, D. C. Barnes, D. P. Brennan, et al., *Phys. Plasmas* **13**, 058103 (2006).
- [53] S. I. Braginskii, “Transport processes in a plasma”, in *Reviews of Plasma Physics*, M. A. Leontovitch, ed., Vol. 1, p. 205 (Consultants Bureau, New York, 1965).
- [54] E. D. Held, J. D. Callen, C. C. Hegna, C. R. Sovinec, T. A. Gianakon and S. E. Kruger, *Phys. Plasmas* **11**, 2419 (2004).
- [55] T. G. Jenkins, S. E. Kruger, C. C. Hegna, D. D. Schnack, and C. R. Sovenic, “Calculating electron cyclotron current drive stabilization of resistive tearing modes in a nonlinear MHD model”, submitted to *Phys. Plasmas* (2009).
- [56] C. C. Kim and the NIMROD Team, *Phys. Plasmas* **15**, 072507 (2008).
- [57] G. Y. Fu, W. Park, H. R. Strauss, J. Breslau, J. Chen, S. Jardin and L. E. Sugiyama, *Phys. Plasmas* **13**, 052517 (2006).